CHAPTER 3: LABORATORY AND FIELD PROGRAMMES

TABLE OF CONTENTS

LIST OF TABLES

LIST OF FIGURES

LIST OF SYMBOLS / ABBREVIATIONS

ACV	Aggregate crushing value
Agg	Dimensionless joint stiffness per unit length of joint/crack;
ARAN	Automatic road analyser
C	Continuous
DC	Discontinuous
$E_{c,28}$	Theoretical 28-day elastic modulus of concrete
FWD	Falling weight deflectometer
$f_{cu,28}$	28-day characteristic cube strength
h	Slab thickness
LTE	Load transfer efficiency
RM	Relative vertical movement at joint
τ	Shear stress at crack face

3 LABORATORY AND FIELD PROGRAMMES

3.1 LABORATORY PROGRAMME

3.1.1 Introduction

The primary objectives of this research project were stated in Chapter 1. Existing methods for modelling aggregate interlock shear transfer to develop a model applicable to South African conditions that reflects variations in joint load transfer with joint opening, load magnitude, subbase support, aggregate size and concrete properties, were investigated through a literature review presented in paragraph 2.4. EverFE (Davids et al., 1998a) was used for three-dimensional finite element modelling as summarised in Appendix D. The difference in jointed concrete pavement response in terms of deflections, to static and moving impulse or dynamic loads (equivalent to traffic loads), has also been pointed out in paragraph 2.3.

Apart from the design guidelines found in Manual M10 (1995) very little was found in the literature that focussed on the aggregate interlock load transfer characteristics of South African crushed aggregates, and under South African environmental conditions.

With the advancement in technology and an ever changing environment, it was logical that more sophisticated methods would be developed for designing pavements. With 3D FE methods it is possible to adequately capture the structural response of pavement systems as they are encountered in the field.

In line with this advancement in technology, a mechanistically based design method for concrete pavements has been developed in South Africa, to facilitate interaction with the mechanistic flexible pavement design methods currently in use, and to promote the use of concrete to rehabilitate flexible pavements.

Suitable models have been developed from finite element and multi-layer evaluations and a user-friendly computer program has been compiled. The design procedure takes into account a large number of input variables, the fact that pavement characteristics change with time, and that the different parameters show statistical variation. All of the above, together with actual field performance, was taken into account in generating an output, which is expressed in terms of risk of failure. The design method has been calibrated against actual performance on various sections and pavement types, such as roads, streets and hard standings.

The insight gained in the mechanics of aggregate interlock at joints/cracks in concrete pavements through the literature review, provided the guidance for the experimental programme followed in the present study as set out in Chapter 2.

As mentioned in Chapter 2, the experimental programme was set up according to a 2-level, 2-parameter design. The aggregate types chosen were Granite with an E-modulus of 27 GPa (Aggregate crushing value (ACV) = 27%), and Dolomite with an E-modulus of 40 GPa (ACV = 15%), representing the range in modulus of crushed aggregates used in the construction industry in South Africa. To cover the spectrum of aggregate sizes used in the construction of concrete, 19 mm as well as 37,5 mm coarse aggregates were used. For this purpose four concrete slabs were cast, as follows:

a) Experiment 1 – 19 mm granite aggregate.
b) Experiment 2 – 37,5 mm granite aggregate.
c) Experiment 3 – 19 mm dolomite aggregate.
d) Experiment 4 – 37,5 mm dolomite aggregate.

Apart form the above mentioned four slabs, a fifth concrete slab with a pre-deformed plastic joint former was also cast to investigate the performance of a different type of joint under both dynamic and static loading. Although this experiment was not part of the original design, it will be pointed out in Chapter 5 how the results from this experiment were used to complete the picture of relative movement (RM) versus load transfer efficiency (LTE) results analysed. This slab was also used to quantify the difference between a continuous (C) and a discontinuous (DC) subbase. Wherever reference is made in the text, hereafter to a plastic joint, it implies the joint with a pre-deformed plastic sheet as joint former.

The following paragraphs cover inter alia the test set-up used for the experiments, materials testing conducted, and practical aspects that needed sorting out to obtain relevant data.

3.1.2 Test set-up

Four slabs (1 800 mm long, 600 mm wide, and 230 mm thick) were cast in the laboratory to investigate aggregate interlock LTE at a joint/crack. The thickness of the slab was specifically chosen to represent the average thickness of jointed concrete pavements in South Africa. The slab thickness also has a direct effect on the radius of relative stiffness (l) of the concrete.

The slabs were cast on approximately 55 mm thick rubber (made up out of three layers of rubber on top of each other). The slabs cast for Experiments 1 and 2 were cast with all three layers of rubber intact, whereas before casting the slabs for Experiments 3 and 4, the top layer of rubber was cut through at mid-length directly beneath the position where the crack was formed. This was in order to simulate a crack propagating into the subbase.

When tested in a California Bearing Ratio (CBR) press to determine the equivalent bearing capacity of the rubber, it was measured as 24% CBR. This is equivalent to a selected gravel layer with a resilient modulus of approximately 150 MPa (Theyse et al., 1996), and a k-modulus of 80 MPa/m. This same subgrade k-value was used in theoretical analyses with EverFE (see Appendix D).

The rubber and shuttering were placed on a timber pack (2 800 mm long, 700 mm wide, and 140 mm thick). The timber pack had to render a sound base for transporting the slab from the position where it was cast to where it was tested. A crack inducer in the form of an angle iron was placed across the floor of the slab at mid-length on the rubber foundation, before casting (see Photos G.1 and G.2). For Experiment 1 a 40 mm deep incision was cut into the concrete surface with a grinder (vertically above the angle iron), where after the desired crack was formed. For Experiments 2, 3 and 4 the incision was formed by casting a flat bar into the top of the concrete slab vertically above the angle iron.

The joint/crack had to be formed within 24 hours after casting the concrete (see Photo G.4). By then the concrete had already set, and was strong enough that the surface would not be damaged, but on the other hand still weak enough that a vertical crack could be induced without applying too much force. With the strength of the cement matrix being weaker than the aggregate at the time of forming the crack, the crack typically formed around the aggregate, with little or no cracked aggregates. This method of cracking the slab also ensured that a coarse aggregate interlock surface was created with little loose particles inside the crack. This was verified after completion of each test by taking the two sections of the slab apart, and attempting to collect the fines that formed through abrasion. Very little loose material could be collected, even after completion of Experiments 1 and 2 where the slabs were subjected to 2 million dynamic load cycles, and it was therefore not considered practical. A schematic layout of the test set-up is given in Figure 3.1.

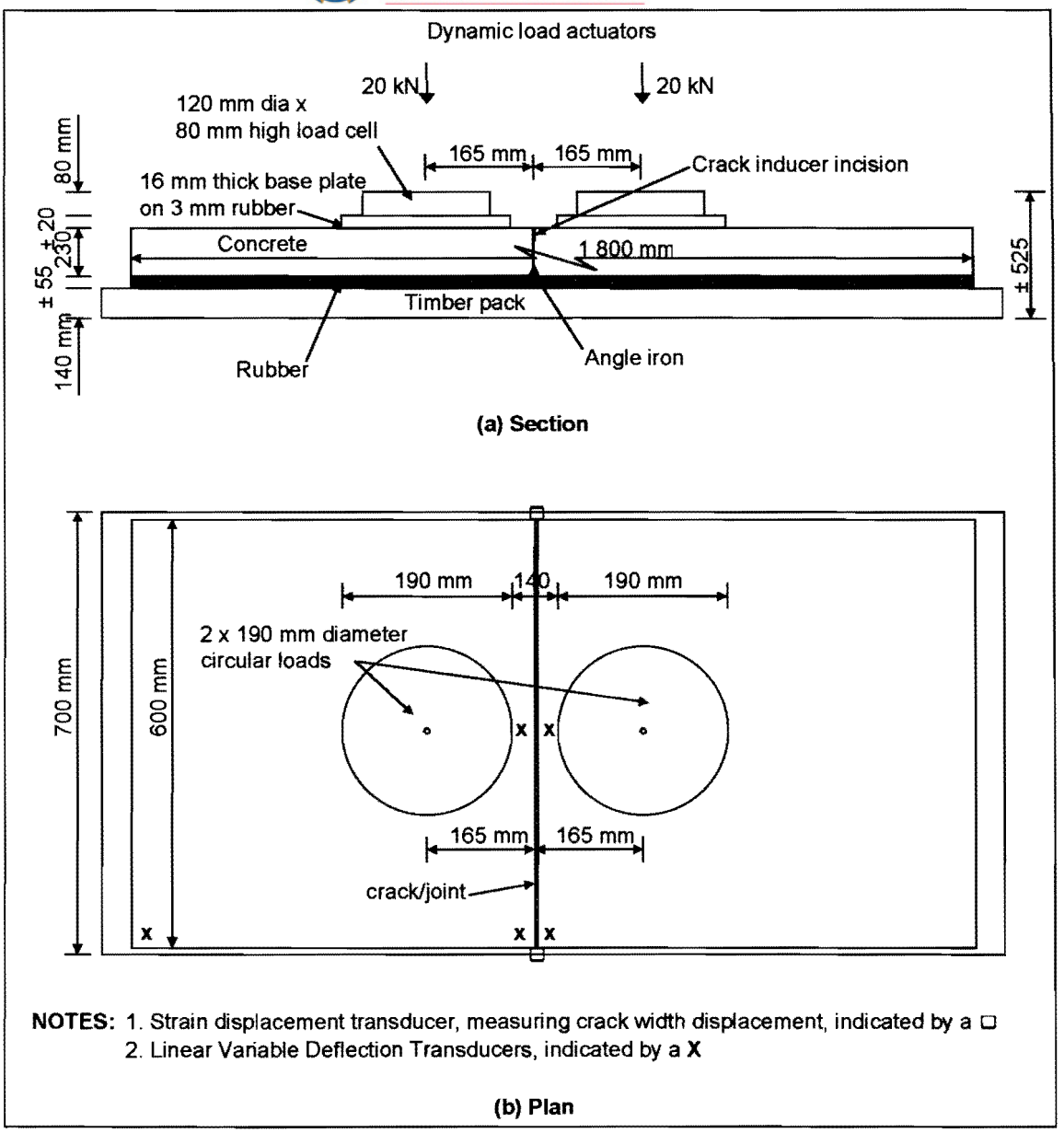

Figure 3.1: Schematic layout of test set-up

3.1.3 Material tests

The slabs were cast, using the materials as summarized in Appendix F. To ensure that a 28-day compressive strength of 35 MPa would be obtained with the materials used, test cubes were made up beforehand, using water/cement ratios of 0,59 and 0,63. The test cubes were crushed after 7 days, and the 28-day strengths were calculated from the assumption that the 7-day compressive strength is approximately two-thirds that of the 28-day compressive strength (Fulton, 1994). The average 7-day compressive strength values obtained for water/cement ratios of 0,59 and 0,63 were 21,5 MPa and 20,5 MPa, respectively, which indicated that the corresponding 28-day compressive strength would be

32,5 MPa and 30,5 MPa. From these results it was determined that a water/cement ratio of 0,56 should be used to obtain a 28-day compressive strength of 35 MPa. The actual strengths obtained are summarised in Table F.13. Only one set of cubes had an average strength of less than 35 MPa at 28 days. These were the 19 mm granite air-cured cubes, which averaged 30 MPa. The water-cured cubes therefore met the required specification. Apart from the slab, a number of cubes, beams and cylinders were also cast for testing purposes, as summarised in Table 3.1 (see Photos, G.3, and G.5 to G.10).

Table 3.1: Basic information on cubes, beams and cylinders cast for testing purposes

Test specimen	Dimensions (mm)	Number	Time of test
Compressive strength cubes (SABS 863: 1994 / ASTM C39/C39M-01, 2001*)	150 x 150 x 150	18	At 7 and 28 days after casting slab, and at end of 2 million load cycles.
Modulus of rupture beams (SABS 864: 1994 / ASTM C133-97, 1997)	750 x 150 x 150	6	At 28 days after casting slab, and at end of 2 million load cycles.
Shrinkage beams (SABS 1085: 1994 / ASTM C426-99, 1999)	300 x 100 x 100	4	Measure gauge length L_0 before casting specimen, and L_1 after 7 days in curing bath. Place in drying oven with temperature 50°C, and relative humidity 25%, and measure L_2 at 48 hour intervals thereafter, until difference in length less than 2μm/100 mm.
Modulus of elasticity cylinders (BS1881: Part 121: 1993 / ASTM C469-94, 1994)	300 x 150 diameter	3	At 28 days after casting.

*NOTE: ASTM test methods give equivalent test results, although the test methods are not necessarily the same.

The volume of 19 mm and 37,5 mm coarse aggregate in both the granite and the dolomite concrete mixes had to be the same, in order to obtain the same aggregate interlock contact areas. In other words, the coarseness of the joint area formed by the 19 mm granite aggregate had to be the same as for the 19 mm dolomite aggregate. The same applied to the 37,5 mm coarse aggregate concrete mixes. To achieve this, the grading of the granite sand and the dolomite sand had to be approximately the same.

Figure F.1 (Appendix F) shows the grading of the sands used in the concrete mixes, within the grading envelope, and Table F.11 (Appendix F) gives a summary of the mix designs used. The volumetric surface texture (VST) of the crack faces of the experimental slabs, as well as crack faces formed during modulus of rupture testing of concrete beams, was used to verify that the crack faces were similar. The methodology followed to obtain the VST of the samples is described in Appendix F.

As mentioned above, granite and dolomite aggregates were chosen as they represented the lowest and highest stiffness moduli, respectively, of the crushed aggregates used in the construction of concrete in South Africa. The results of the cubes, beams and cylinders tested are summarised in Table F.13

(Appendix F). The strength of the aggregate, as well as the size of the aggregate had an effect on the modulus of elasticity results obtained for the four concrete mixes (see Table 3.2). For both the granite and dolomite concrete mixes, the larger sizes coarse aggregate had higher elastic moduli.

The theoretical 28-day elastic modulus, $E_{c,28}$, was calculated using the actual 28-day concrete cube strength obtained in the laboratory, instead of the 28-day characteristic cube strength ($f_{cu,28}$) of 35 MPa (according to the mix design) (Fulton, 2001). This was in order to facilitate a more realistic comparison with what was physically measured in the laboratory. Both 19 mm coarse aggregate concrete mixes had lower elastic moduli than the theoretically calculated moduli. On the other hand, both 37,5 mm coarse aggregate concrete mixes rendered elastic moduli higher than the theoretical values. This in turn indicated that not only the aggregate type, but also the aggregate size, has an influence on the elastic modulus of the concrete.

Table 3.2: Elastic modulus of the concrete – comparison between laboratory results and theoretical results

Aggregate type	Laboratory E (GPa)	$E_{c,28} = K_0 + \alpha f_{cu,28}$ (Fulton, 2001)		
		K_0 (GPa)	α (GPa/MPa)	Calculated E (GPa)
Granite – 19 mm	21,0	17 – 18	0,25	26,5 – 27,5
Granite – 37,5 mm	29,0	17 – 18	0,25	28,0 – 29,0
Dolomite – 19 mm	41,0	24 – 25	0,45	42,5 – 43,5
Dolomite – 37,5 mm	48,0	24 – 25	0,45	43,5 – 44,5

3.1.4 Dynamic loading

The Falling Weight Deflectometer (FWD) measuring instrument is commonly used to determine deflection LTE at a joint in a concrete pavement. With the FWD, dropping a load onto the pavement on the one side of a joint/crack, and measuring the deflection at both sides apply a static impulse load. The deflection LTE is then calculated using Equation (2.4). In practice, however, the loads applied to a pavement are not "one-sided", but dynamic loads are transferred from one slab to the next under moving vehicle traffic. The response of the slabs therefore had to be captured under dynamic loading as well as under static loading to be able to capture real-life conditions and to compare the results.

When subjecting the slab to a simulated dynamic load, it was logical that there would not only be vertical downward forces acting across the crack, but also horizontal forces due to the effects of moment and inertia induced across the crack (see paragraph 2.3). The effect of horizontal forces acting across the crack were controlled by controlling the crack width.

An impulse force that simulates the impact of one wheel (20 kN) of a standard 80 kN dual wheel truck axle load, crossing a joint/crack at 80 km/h, was developed. This was achieved by using two actuators. The first actuator had to simulate a wheel approaching the crack by increasing the applied load from zero to 20 kN within 0,11 seconds. The load on the leave slab was then released to zero in 0,01 seconds. In this same 0,01 second interval that the first actuator reverted back to zero, the second actuator had to move from zero load to 20 kN load on the approach slab, where after it was released back to zero in 0,11 seconds to simulate a wheel moving away from the crack. This action was followed by an interval of approximately 0,11 seconds when there was no load on either actuator, and the slabs returned to a no-load position. The two waveforms thus created had a total duration of 0,12 seconds each, with a rest period of 0,11 seconds (corresponding to approximately 3 Hz), as shown in Figure 3.2. These waveforms were similar to the ones used by Colley and Humphrey (1967), but at approximately twice the speed.

It was initially planned to conduct testing in a standard MTS, using one actuator with a load arm on a hinge. This meant that the actuator had to apply a 20 kN compressive force, move through zero force, and apply a 20 kN tensile force within 0,01 seconds. This however was not possible, as the actuator load cell became unstable when it went through zero, and the tensile force values could not be controlled. Two actuators were therefore used to apply the load waveforms.

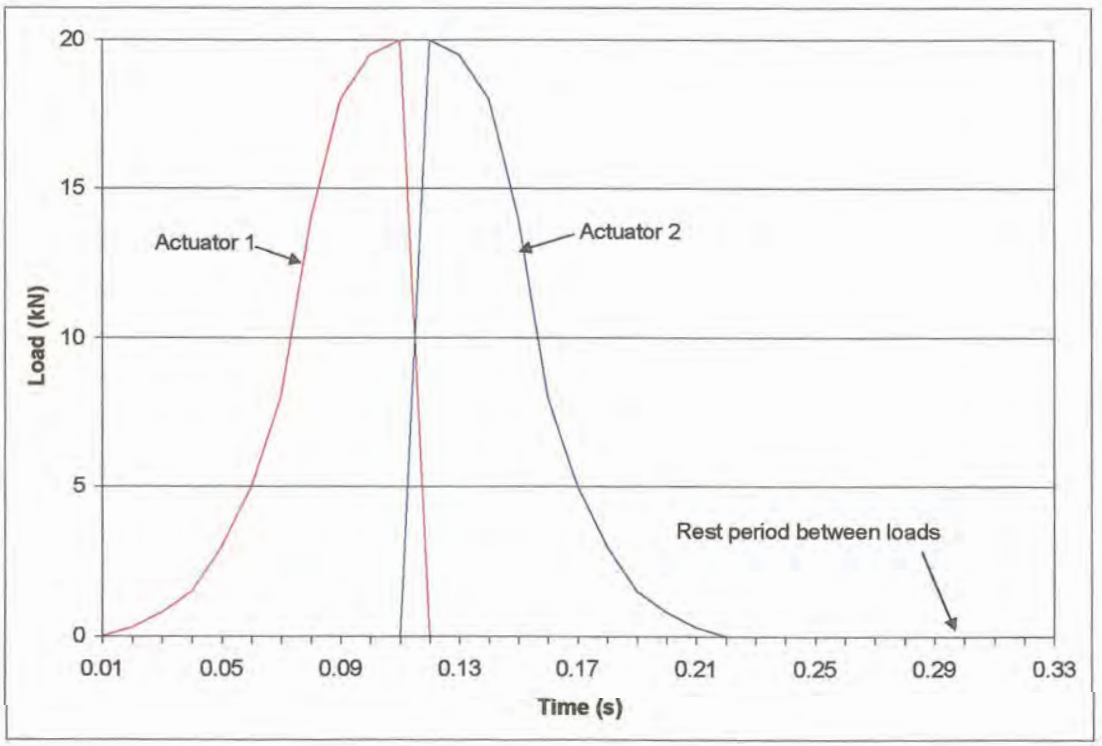

Figure 3.2: Typical load waveforms for dynamic loading

3.1.5 Test procedure

During Experiment 1 a total of 15 data channels were recorded continuously on a computer using HBM KWS and HBM Spider-8 amplifiers (see Photo G.11), namely:

- 2 Load cells
- 2 Actuators
- 1 Actuator deflection
- 5 Linear Variable Displacement Transducers (LVDT's)
- 2 Strain Displacement Transducers
- 3 Thermocouples

Measuring the loads applied, as well as the deflections induced during dynamic loading necessitated accurate measuring equipment. The deflection measuring devices, especially, had to be accurate to at least 0,1 μm, as the magnitude of the expected deflections (obtained from the theoretical modelling in Appendix D) was expected to be between 0,0 mm and 1,0 mm.

As indicated in Figure 3.1, the two load cells were placed at positions, determined by the load waveforms induced by the two actuators to simulate a wheel crossing the crack at 80 km/h. The deflection of the actuator on the leave slab was also measured. Two LVDT's were positioned on opposite sides of the crack in the centre of the slab between the load cells to measure deflections in the wheelpath. Another two LVDT's were placed on opposite sides of the crack on the edge of the slab to determine the deflections at the edge, and one LVDT was placed in an outside corner of the slab to measure the movement that took place away from the crack. The fifth LVDT in the outside corner of the slab was also used as a control to ensure that the ends of the slab did not lift up. For Experiment 1 only two strain displacement transducers were fixed on both sides of the slab at the top of the crack, but for further experiments this number was increased to four in order to be able to measure horizontal opening and closing movements at the top as well as at the bottom of the crack. The total number of data channels logged was therefore increased to 17.

The thermocouples were read every 30 minutes. All other data channels were logged continuously during the dynamic loading process. This created a large data file. In order to save file space only data from 2 load cycles at 1-minute intervals were sampled and saved to a smaller file for analysis purposes.

3.1.6 Experimental programme

As mentioned above, there were practical aspects of the experimental procedures that needed sorting out during the first experiment. Initially the intention was to subject all four concrete slabs to at least 2 million dynamic load cycles. It was reasoned that it would be possible to measure deterioration of the

crack face through a decrease in deflection measurements. The slab cast for Experiment 1 was therefore subjected to 2 million dynamic load applications. After every 0,5 million load applications, static loading tests were carried out, and the data analysed to determine general trends. The equipment was also calibrated at the time of static load testing.

Figure 3.3 presents typical deflection data obtained for the 1,5 to 2 million load cycles that the first slab was subjected to at the initial crack width of 0,1 mm. There was no significant deterioration of the crack up to 2 million dynamic load cycles, which indicated that both the cement paste and aggregate particles were so tightly knit together that little vertical sliding could occur (Benkelman, 1933). On the other hand, while applying the dynamic loads, the crack width was also monitored continuously. The relative horizontal opening movement at the crack did increase during application of the 2 million dynamic load applications, yet when the load was removed the actual crack width stayed at 0,1 mm.

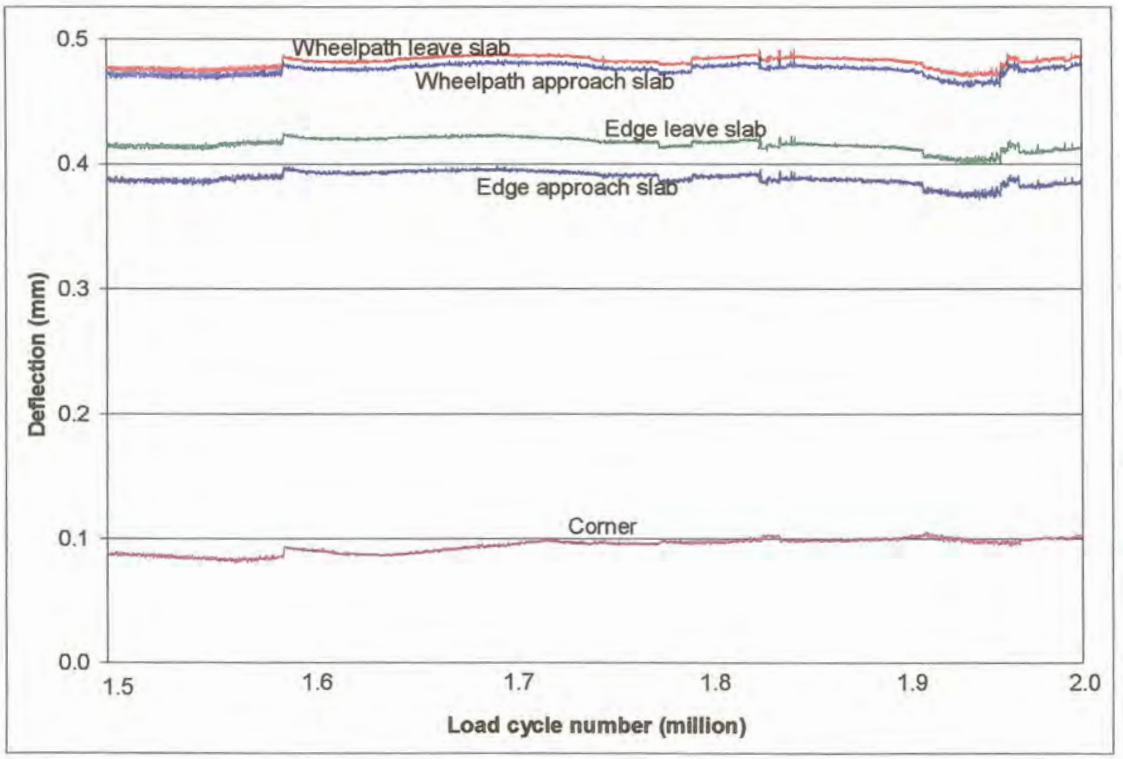

Figure 3.3: Deflection measurements – 1,5 to 2 million dynamic load cycles at 0,1 mm crack width

This indicated that little abrasion of the aggregates at the joint face took place at the initial crack width, as the narrow crack restricted vertical shear movement. Therefore no loose particles were dislodged, or got trapped in a different position when the crack opened and closed. This could also be attributed to the high quality of crushed stone used in South Africa (see Appendix F), and to the time that the crack was formed, as the cement matrix was still soft enough not to splinter off.

To test the above statements, the slab cast for Experiment 2, using 37,5 mm granite aggregate in the concrete was also subjected to 2 million dynamic load cycles, with static load tests and calibration of equipment after every 0,5 million load cycles. Once again there was no significant deterioration of the concrete at the crack face, and the crack width also did not increase. The further implication was that it was not necessary to allow so much time (18 days for Experiment 1) for dynamic load testing at the initial crack width, but that testing at different crack widths could commence as soon as the test set-up was complete. Other factors that had to be borne in mind, were that testing was conducted inside a laboratory building, and that the slab was not subjected to normal day-night temperature variations, nor exposed to rain, and other environmental effects detrimental to a joint in a concrete pavement.

Another explanation could be that the shear stress on the crack face at the initial crack width was too low due to lack of support from the rubber subbase. The shear stress at the crack face was therefore calculated using the following equation:

$$\tau = \frac{Agg(RM)}{h} \tag{3.1}$$

Where:

τ	=	Shear stress (MPa);
Agg	=	Dimensionless joint stiffness per unit length of joint/crack;
RM	=	Relative vertical movement at joint (mm); and
h	=	Slab thickness (mm)

The shear stress at the crack face during the initial 2 million dynamic load cycles was calculated as 0,32 MPa for Experiment 1 and as 0,21 MPa for Experiment 2. These results were low in comparison with both the 28-day compressive strength results, as well as with the elastic modulus results. As mentioned previously the equivalent k-value of the rubber subbase was 80 MPa/m. It was therefore not that the support was not stiff enough, but due to the fact that high LTE's with low RM's were measured during the dynamic loading.

After completion of the dynamic loading cycles the two sections of the slab were pulled apart horizontally in a controlled fashion, to measure responses under static and dynamic loading at different crack widths. However, before pulling the two sections of the slab apart at the crack, the ends of the slab were pressed down by inserting jacks beneath the steel frame holding the actuators. This was done in order to ensure that the aggregate interlock bond that still existed across the crack was broken, in order to be able to pull the two sections apart (see Photos G.12 to G.15).

Following on the conclusion already reached from the first two Experiments, that little or no deterioration of the crack face occurred at the initial crack width during loading, the slabs cast for Experiments 3 and 4 were not subjected to the 2 million dynamic load cycles applied to the first two slabs. The focus was therefore shifted from determining the effect of abrasion under repeated dynamic

loading to determining the response of the concrete at different crack widths. The slabs for Experiments 3 and 4 were therefore subjected to only three cycles of 10 minutes of dynamic loading, followed by static loading at the initial crack width. Thereafter, as for the previous two experiments the two sections of the slab were pulled apart and subjected to dynamic and static loading at different crack widths. The slabs were pulled open and tested at different crack widths up to a maximum crack width of 2,5 mm to be on par with similar studies researched during the literature survey (Davids et al., 1998). The slabs were then pushed together again to as close as possible to the initial crack width, and pulled open again, at least three times to verify the repeatability of the tests.

These opening and closing cycles to a maximum crack width of 2,5 mm were conducted for all the experiments (see Photos G.17 and G.18), except for Experiment 3 that was pulled open to a maximum crack width of 4,0 mm. This was in order to test the assumptions of previous researchers that at crack widths greater than 2,5 mm the deflection measurements reached an upper asymptote. 2,5 mm was also considered the crack width at which the subbase started to play an important role in the LTE of the concrete pavement system (Colley and Humphrey, 1967; Davids et al., 1998b; Jensen, 2001). Figure 3.4 illustrates this upper plateau reached in the deflection measurements, and confirmed that testing up to a crack width of 2,5 mm was sufficient to measure the effects of aggregate interlock. At least for 19 mm coarse aggregate concrete.

As mentioned above, a major difference between Experiments 1 and 2, and Experiments 3 and 4 was that the top layer of rubber beneath the concrete was cut through at mid-length directly beneath the joint for the latter, but that all three layers of rubber were left intact for the former.

3.2 AGGREGATE INTERLOCK EXPERIMENTS

The following paragraphs present a chronological description of the testing done in order to collect the data necessary for analysis purposes. Each experiment is described separately with specific reference to deflection measurements, horizontal crack displacement, LTE, and RM. Where appropriate comparisons are also made with a combination of results from more than one experiment. Some observations on the general behaviour of the slabs during testing, as well as the effect of temperature cycles are also presented.

EverFE is also plotted on the graphs. As mentioned above, the larger RMs calculated with EverFE, resulting in lower LTEs did not compare well with the experimental results. The relative vertical movement at the joint for both coarse aggregate sizes considered was calculated using Equation (2.12). The values of the line plotted for 37,5 mm coarse aggregate was initially lower than the laboratory values, but the line increased exponentially with increasing crack width, to values higher than what was measured. The main concern, however, was the large difference between the experimental results and the line plotted for 19 mm coarse aggregate using values calculated with Equation (2.12) (Figure 3.15) The magnitude of the difference in results is more obvious when comparing the scale of the vertical axes of Figures 3.15 and 3.16. The former has a maximum value of 3,5 mm, versus the 0,35 mm of the latter.

From Figure 3.15 it is obvious that Equation (2.12) that was still incorporated as one of the design parameters in Manual M10 (1995) was inaccurate and needed revision.

3.2.3 Experiment 3

The slab cast for Experiment 3, using 19 mm dolomite aggregate (see Photo G.21), was subjected to three cycles of 10 minutes of dynamic loading followed by static loading at the initial crack width. Thereafter, as for the previous two experiments the two sections of the slab were pulled apart and subjected to dynamic and static loading at different crack widths. The slab was pulled open and tested at different crack widths up to a maximum crack width of 4,0 mm, closed back to the initial crack width and pulled open again. This procedure was done at least three times to verify the repeatability of the tests.

One major difference between Experiment 3 and Experiments 1 and 2 was that the top layer of rubber beneath the concrete was cut through directly beneath the joint. This was to simulate a crack projecting into the subbase, and test the assumption made previously that the high LTE obtained for Experiments 1 and 2 was partly due to the continuous support provided by the rubber subbase. The fact that the top layer of rubber was cut through necessitated that the mechanisms by which the opening and closing of the slab were performed be more closely controlled, as the possibility existed that the top layer of rubber could slide off during opening of the crack.

The increase in deflection with increasing crack width for both dynamic and static loading is shown in Figure 3.17. When comparing this figure with Figure 3.5, it is obvious that in Experiment 3, the deflections measured were far less than what was measured for Experiment 1. On the other hand, the results were less than the theoretical predictions from EverFE, but within a factor of 10 of the results reported by Jensen (2001). The dynamic loading results were on average 124% that of the static loading results. This was similar to results reported by Bergan and Papagiannakis (1984).

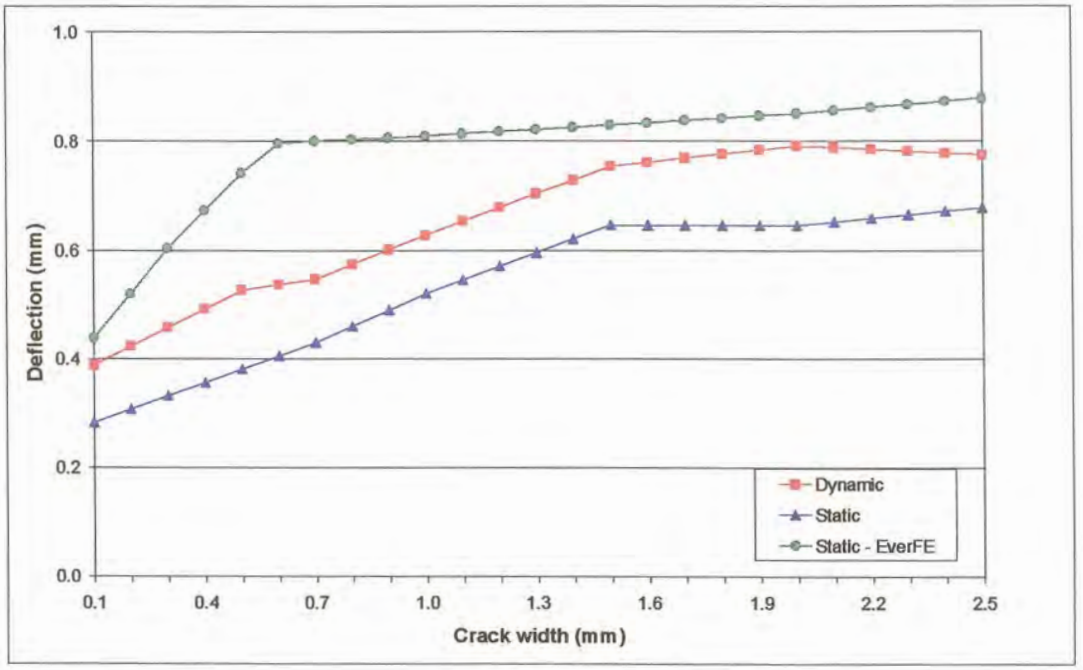

Figure 3.17: Deflection (of leave slab) versus crack width (19 mm dolomite aggregate)

The development of horizontal crack displacement at different crack widths is plotted on Figures 3.18 and 3.19 for dynamic and static loading, respectively. For comparison purposes the scale of the vertical axes have been kept constant (see also Figures 3.6, 3.11 and 3.12). Once again, it was noticeable that larger horizontal movements occurred as the crack started to open up at a crack width of 0,5 mm.

Both Experiments 1 and 3 contained 19 mm coarse aggregate, although from different sources, namely granite and dolomite aggregate, respectively. The deflection LTE graphs obtained for these two Experiments are plotted on Figure 3.20. The theoretical line determined with EverFE is also plotted on the graph for comparison purposes.

The deflection LTE obtained for the 19 mm dolomite (Experiment 3) was less than what was previously calculated for the 19 mm granite (Experiment 1). As it has already been established through VST testing (see Appendix F) that the crack faces of these two slabs were similar, this difference in results could be attributed to the fact that in the case of Experiment 3, the top layer of the rubber supporting the concrete was cut through directly beneath the joint/crack position. This simulated crack into the subbase therefore inhibited the transfer of shear stresses, thereby reducing the efficiency of the system. As previously, the theoretical LTE determined with EverFE was initially close to a 100%, but at a crack width greater than 0,5 mm, it decreased to values considerably lower than what was calculated from the laboratory results. The apparent explanation for this difference has been dealt with in paragraphs 3.2.1 and 3.2.2, above.

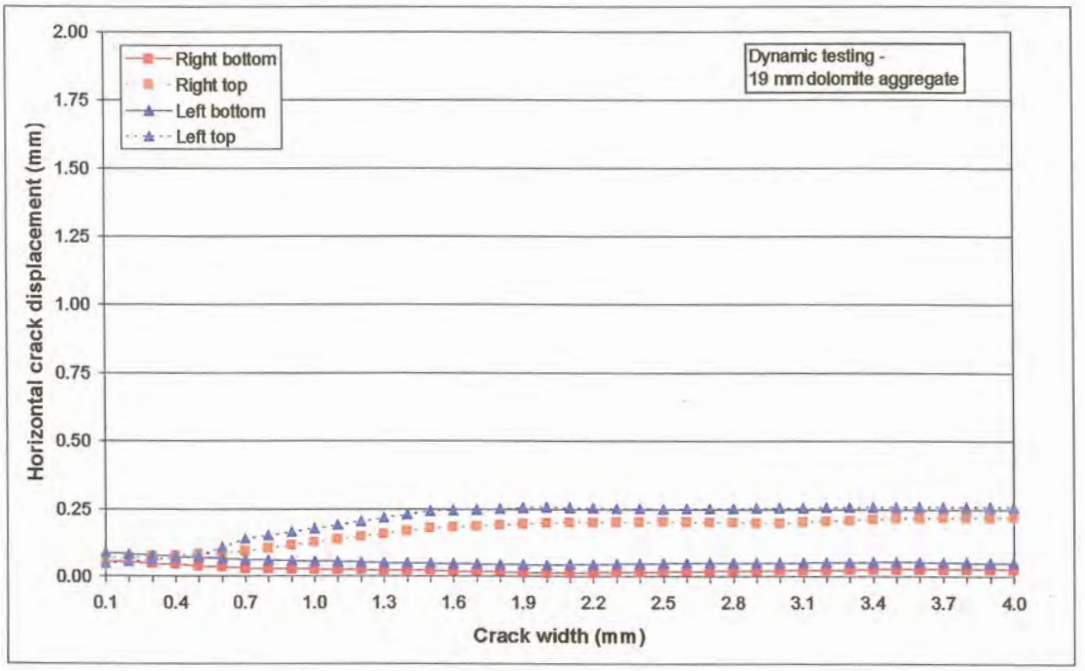

Figure 3.18: Horizontal crack displacement versus crack width under dynamic loading (19 mm dolomite aggregate)

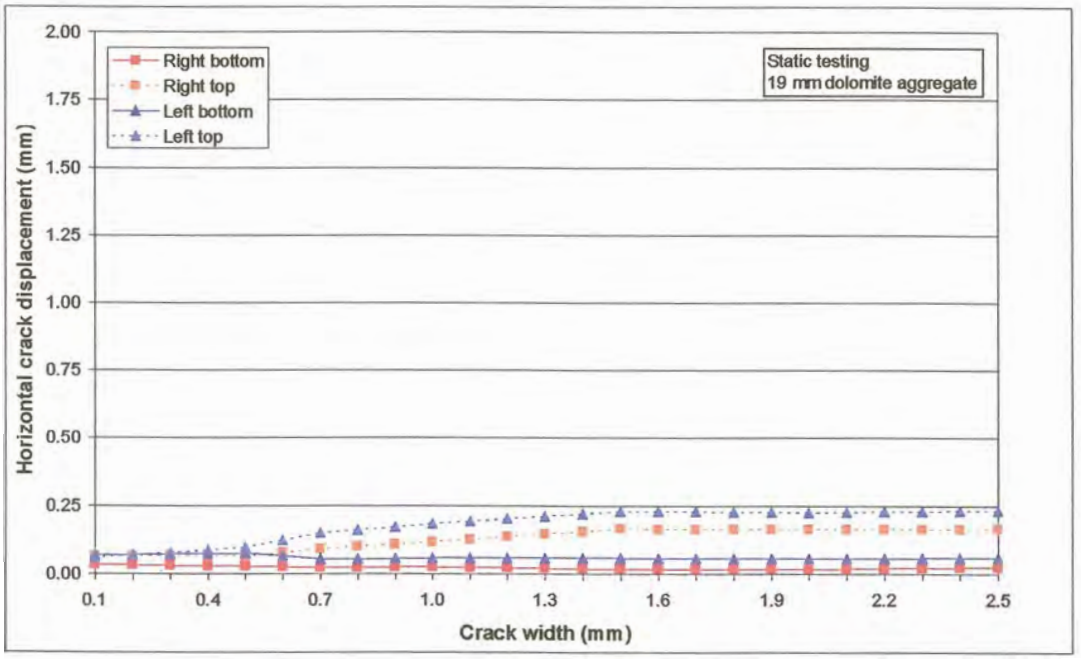

Figure 3.19: Horizontal crack displacement versus crack width under static loading (19 mm dolomite aggregate)

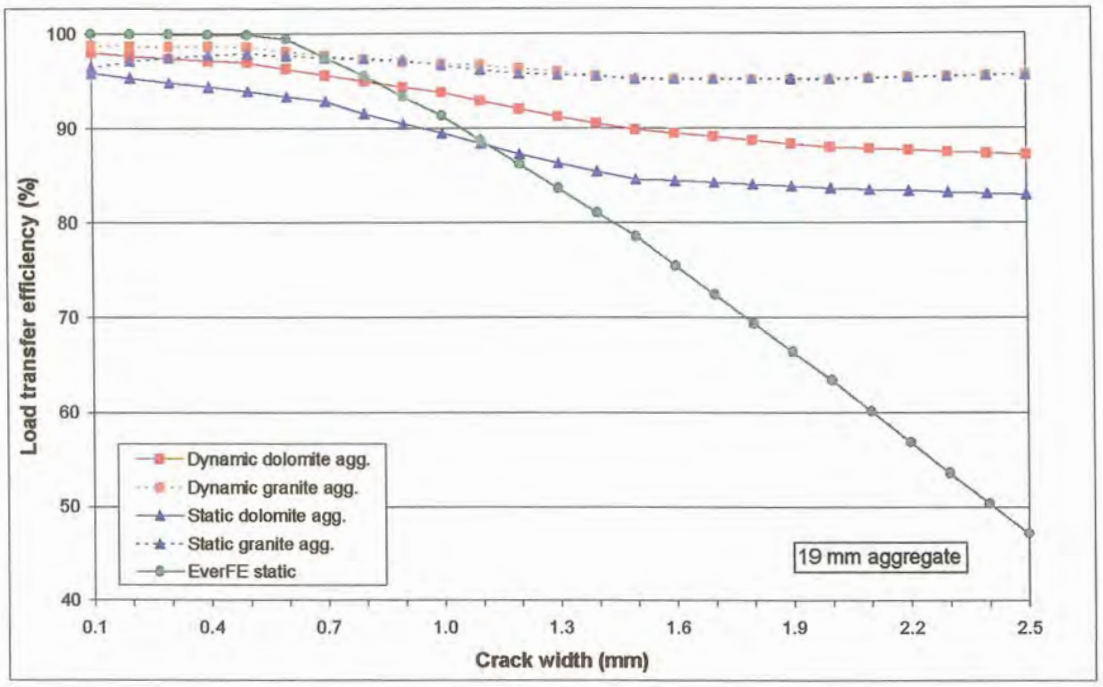

Figure 3.20: Deflection LTE versus crack width – 19 mm aggregate

When the results obtained on the granite and dolomite were compared in terms of RM, the results were almost the same. The average of the RM results of the 19 mm granite aggregate and the 19 mm dolomite aggregate was therefore calculated. The logistic model was used to fit the data as the dependent variables showed dichotomous (two-value or high-low) behaviour. The software package Mathcad 2000 (Version 8) was used to fit the data in terms of RM (y) and crack width (x), as follows:

Dynamic loading:

$$y(x) = \frac{0{,}103}{1 + 22{,}375 \cdot e^{-2{,}639x}}; \qquad R^2 = 96{,}9\% \tag{3.2}$$

Static loading:

$$y(x) = \frac{0{,}114}{1 + 18{,}644 \cdot e^{-2{,}609x}}; \qquad R^2 = 96{,}5\% \tag{3.3}$$

For both curves, the R-squared value, also known as the coefficient of determination, was used as an indicator of how closely the estimated values for the logit functions corresponded to the actual data. A fitted function is most reliable when its R-squared value is at or near 1. Figure 3.21 show the curves fitted for the logistic equations (logit) of both dynamic and static loading, together with the experimental data.

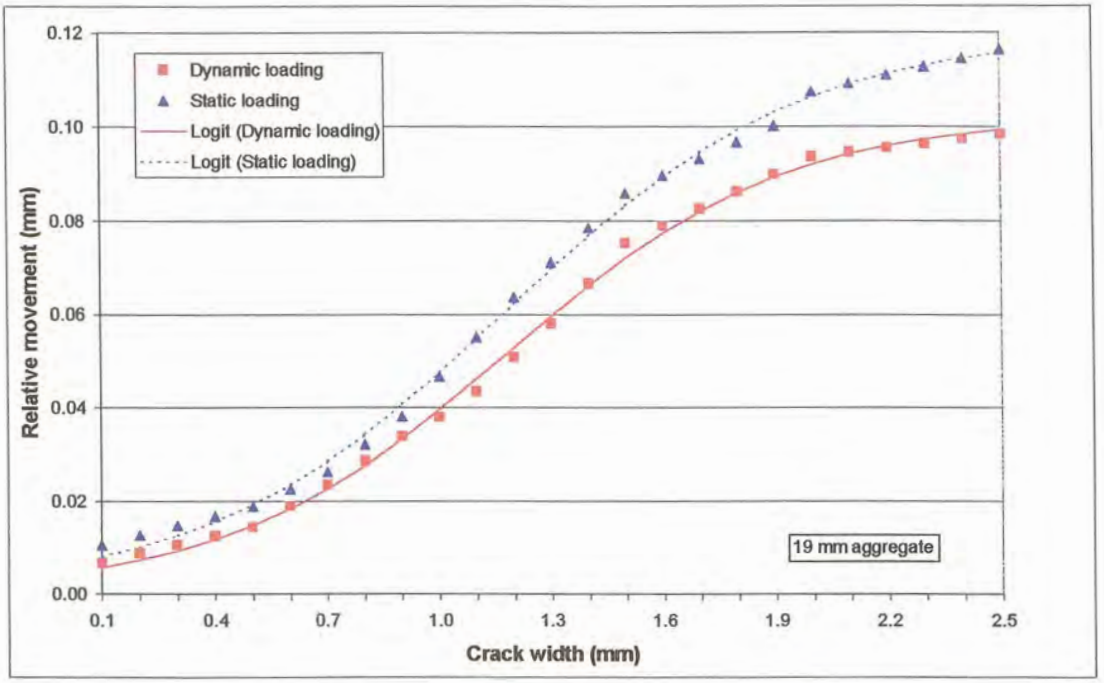

Figure 3.21: Average of RM versus crack width results for dynamic and static loading on 19 mm granite and dolomite aggregate

Evaluating the aggregate interlock efficiency of the joint in terms of RM is contrary to the generally accepted method of determining the efficiency of a joint in terms of deflection LTE, but similar to the method used by Strauss (1992), as well as by Strauss et al. (2001). Strauss (2001) considered that evaluating the efficiency of a joint in terms of deflection LTE is not necessarily the correct method, as it gives results based on the efficiency of the whole system. In other words, it not only takes into account the deflection of the concrete slab, but also indirectly the deflection of the subbase and subgrade. On the other hand, when analysing the RM measured on top of the concrete, the deflection of the concrete is isolated.

However, this approach is not logical as there are three components involved during load transfer at a joint/crack, namely: the portion carried by the slab, the portion carried by the subbase/subgrade, and the portion carried by the load transfer mechanism. These components have to be in equilibrium, and during the measurement of LTE, if one carries more of the imposed load, the others will carry less.

On completion of the initial set of dynamic and static tests at different crack widths, the steel frame holding the actuators was turned 90 degrees. This was in order to apply a 40 kN (the 2 actuators adjacent to each other) static load on the one side of the joint/crack. The results were then compared to those previously obtained under 20 kN static loading.

Due to the repeated cycle of opening and closing the two parts of the slab during initial testing, some particles were loosened on the crack face, which prevented closing the crack to less than 1,0 mm. Results under 40 kN load application were therefore only obtained for crack widths between 1,0 mm and 2,5 mm. Figure 3.22 shows the deflection versus crack width measured on the leave slab for both 20 kN and 40 kN static loading, with the deflection under the heavier load 40 kN load on average 19% higher than under the lighter 20 kN load.

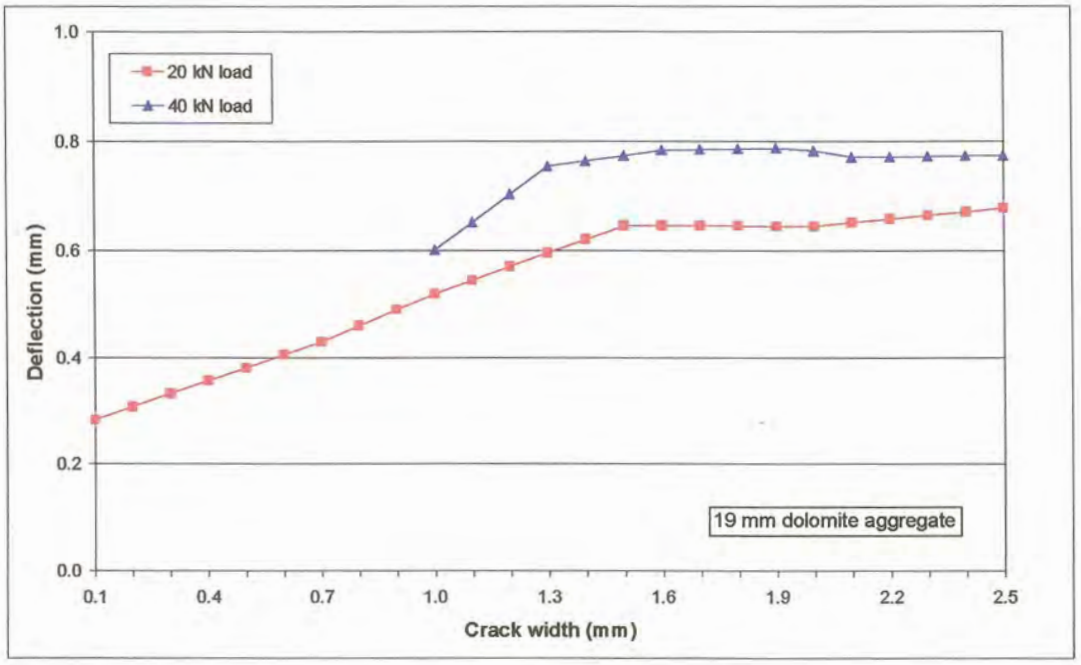

Figure 3.22: Deflection (of leave slab) versus crack width for 20 kN and 40 kN static loading (19 mm dolomite aggregate)

The deflection LTE in the wheelpath obtained for the 19 mm dolomite aggregate, subjected to both 20 kN and 40 kN static loads, is plotted on Figure 3.23. The deflection LTE lines plotted for the 20 kN and 40 kN loads were approximately parallel to each other, with the 40 kN loading results on average 2% higher than the values for the 20 kN load. Considering the magnitude of the deflections, this difference in results is negligible.

Similarly, the RM measured beneath 20 kN static loading, was compared with the RM measured beneath 40 kN static loading, and is plotted on Figure 3.24. The RMs calculated from the 40 kN loading results were 5% lower than those calculated for 20 kN loading. Despite the fact that the 40 kN load caused higher deflections at the crack than the 20 kN load, the relative deflection/movement between the leave slab and the approach slab was smaller. This was primarily due to the 40 kN load transferring larger forces across the crack than the 20 kN, and therefore the smaller RM. Once again the magnitude of the difference is remarkably small.

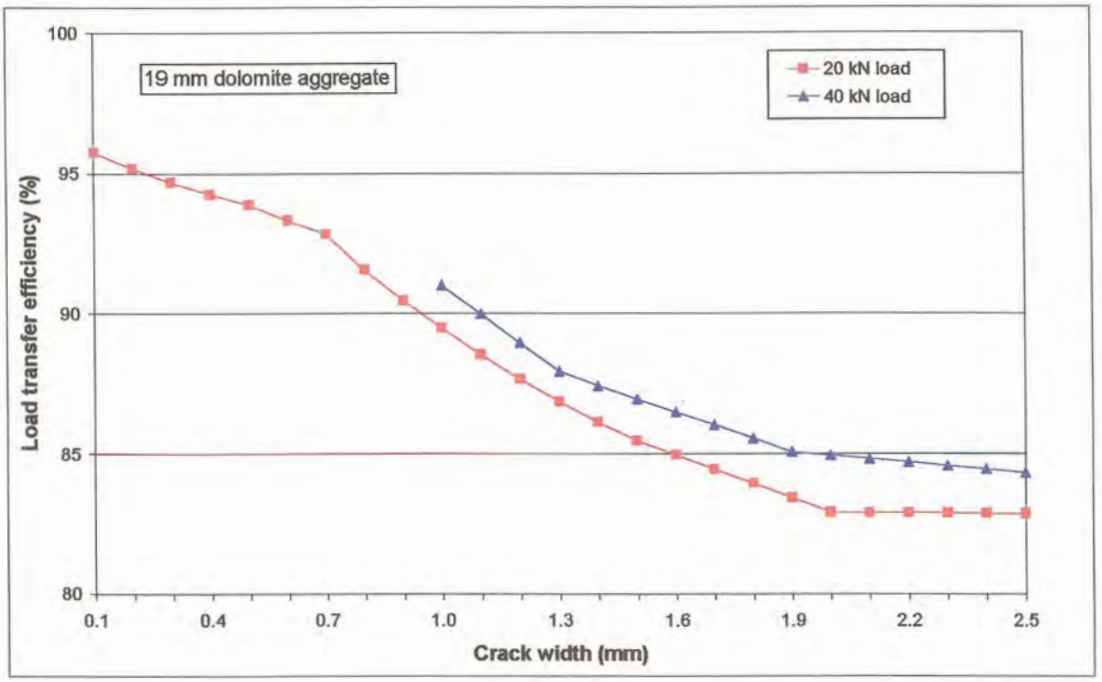

Figure 3.23: Deflection LTE – 20 kN versus 40 kN static loading (19 mm dolomite aggregate)

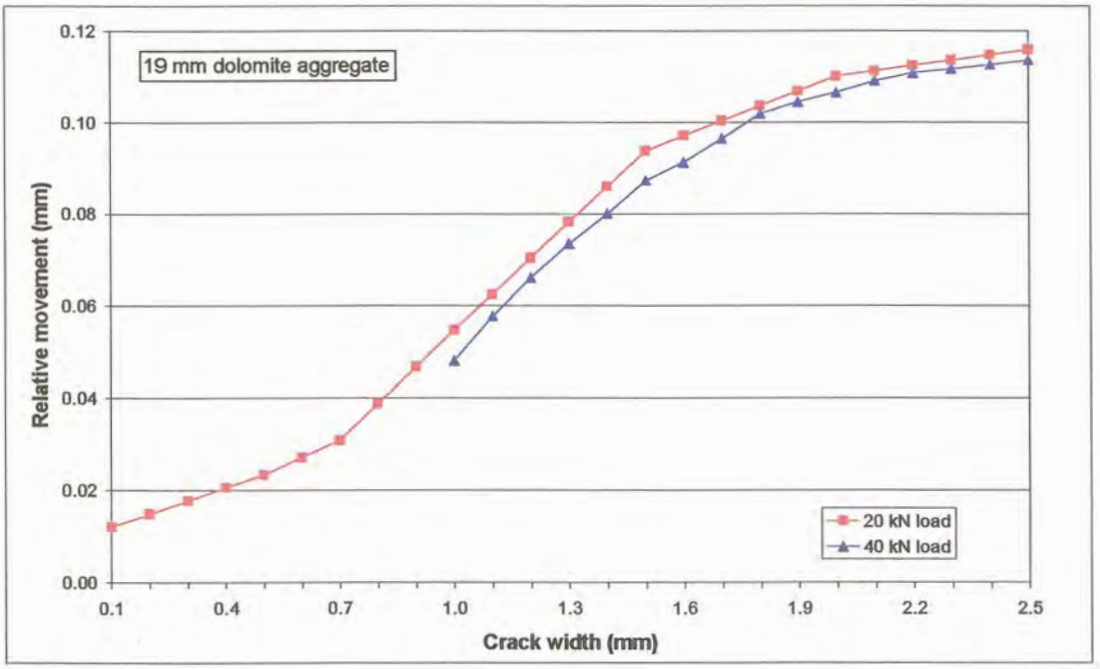

Figure 3.24: RM at joint – 20 kN versus 40 kN static loading (19 mm dolomite aggregate)

3.2.4 Experiment 4

The slab cast for Experiment 4 contained 37,5 mm dolomite aggregate (see Photo G.22). Similar to Experiment 3, this slab was also subjected to three cycles of 10 minutes of dynamic loading followed by static loading at the initial crack width. Thereafter, the two sections of the slab were pulled apart and subjected to dynamic and static loading at different crack widths. The slab was pulled open and tested at different crack widths up to a maximum of 2,5 mm, closed back to the initial crack width, and pulled open again, at least three times to verify the repeatability of the tests.

As for Experiment 3, the top layer of rubber beneath the concrete was cut through directly beneath the joint to simulate a crack projecting into the subbase. The results of Experiment 4 with 37,5 mm dolomite aggregate were compared with that of Experiment 2, where 37,5 mm granite aggregate was used. This was also in order to test the assumption made previously that the high LTE obtained for Experiments 1 and 2 was partly due to the continuous support provided by the rubber subbase

The increase in deflection with increasing crack width for both dynamic and static loading is shown in Figure 3.25. When comparing this figure with Figure 3.13, it is obvious that in the latter case, the deflections measured were less than what was measured for Experiments 1 and 2. Once again the results were also less than the theoretical predictions from EverFE, but similar to the results reported by Jensen (2001). The dynamic loading results were on average 140% that of the static loading results. This was similar to results reported by Bergan and Papagiannakis (1984).

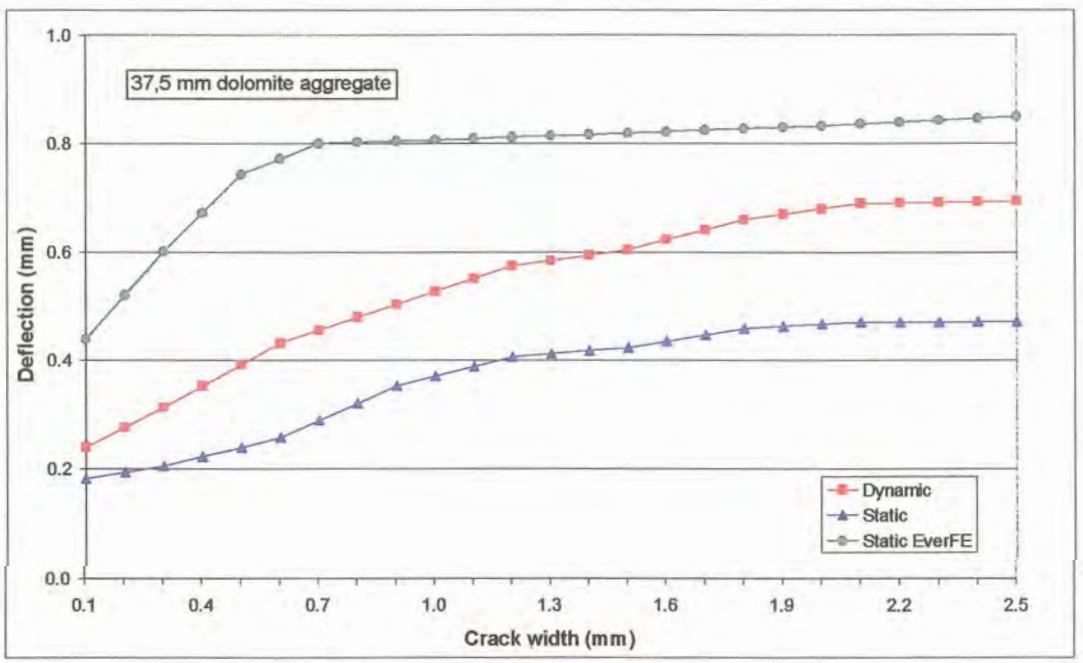

Figure 3.25: Deflection (of leave slab) versus crack width (37,5 mm dolomite aggregate)

The development of horizontal crack displacement at different crack widths is plotted on Figures 3.26 and 3.27 for dynamic and static loading, respectively. For comparison purposes the scale of the vertical axes have been kept constant (see also Figures 3.6, 3.11, 3.12, 3.18 and 3.19). The horizontal displacement at the top of the crack was larger under dynamic loading than under static loading, and also larger than the results plotted for Experiment 3 (Figures 3.18 and 3.19) with the 19 mm dolomite aggregate. In this particular instance the crack tended to open up at the top from smaller crack widths than measured during Experiment 3.

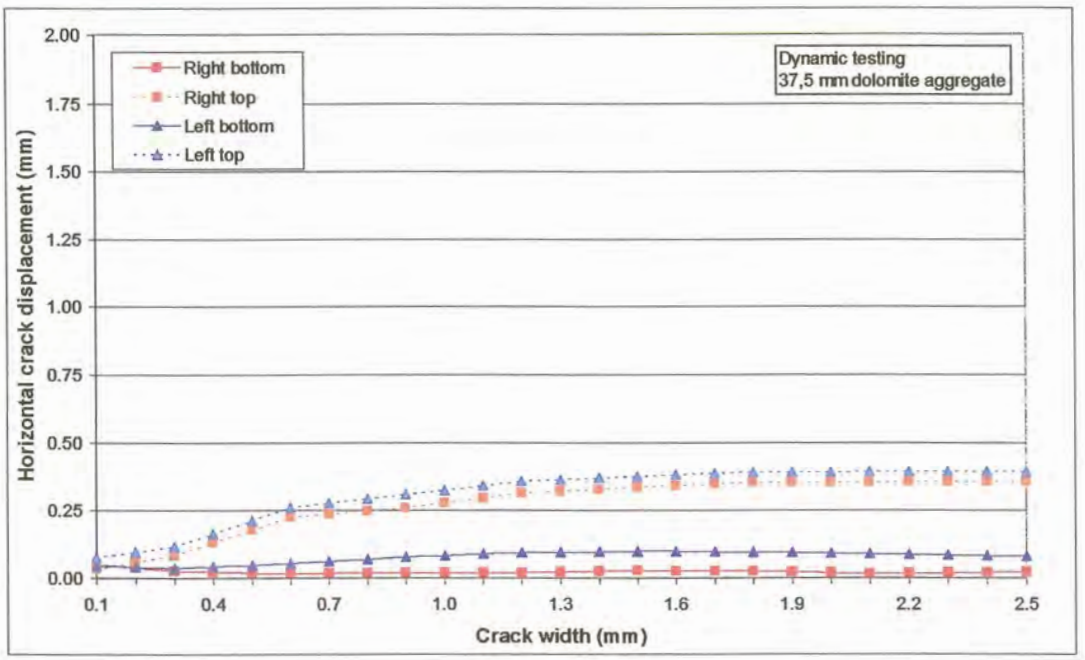

Figure 3.26: Horizontal crack displacement versus crack width under dynamic loading (37,5 mm dolomite aggregate)

Both Experiments 2 and 4 contained 37,5 mm aggregate, although from different sources. Experiment 2 contained, granite and Experiment 4, dolomite aggregate. The deflection LTE graphs obtained for these two Experiments are plotted on Figure 3.28. As for the 19 mm aggregate, it has also been established through VST testing (see Appendix F) that the crack faces of these two slabs were similar. The difference in results could once again be attributed to the fact that in the case of Experiment 4, the top layer of the rubber supporting the concrete was cut through directly beneath the joint/crack position. This simulated crack into the subbase therefore inhibited the transfer of shear stresses, thereby reducing the efficiency of the system. As previously, the theoretical LTE determined with EverFE was initially close to a 100%, but at a crack width greater than 0,5 mm, it decreased to values considerably lower than what was calculated from the laboratory results. The apparent explanation for this difference has been dealt with in paragraphs 3.2.1 and 3.2.2, above.

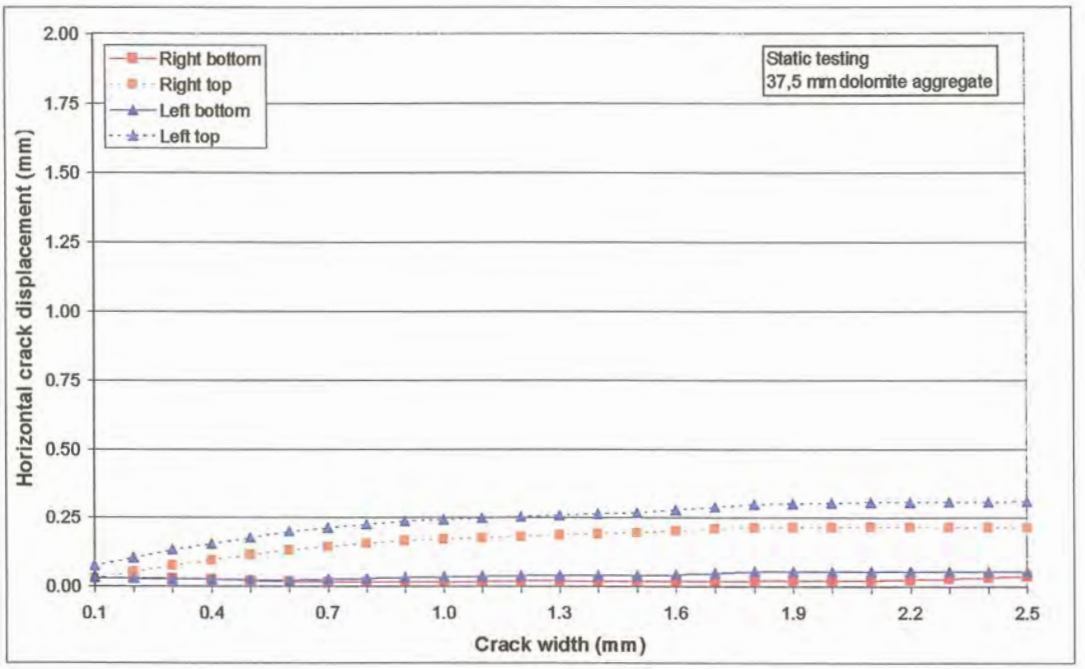

Figure 3.27: Horizontal crack displacement versus crack width under static loading (37,5 mm dolomite aggregate)

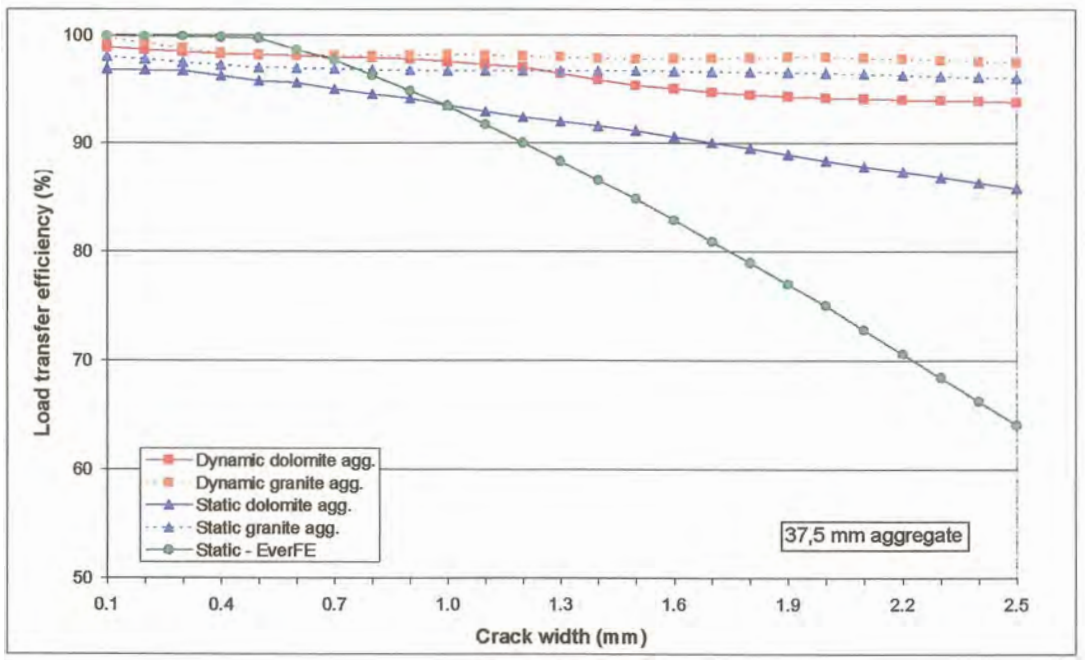

Figure 3.28: Deflection LTE versus crack width – 37,5 mm aggregate

The forces applied to the slab across the crack still rendered higher load transfer efficiencies for dynamic loading than for static loading due to the effect of momentum.

On comparison of the RM results obtained on Experiments 2 and 4, the results were also approximately the same. The software package Mathcad 2000 (Version 8) was used to do a logistic regression on the averages of the dynamic and static loading data in terms of RM (y) and crack width (x), as follows:

Dynamic loading:

$$y(x) = \frac{0{,}060}{1 + 27{,}857 \cdot e^{-2{,}213x}}; \qquad R^2 = 98{,}6\% \tag{3.4}$$

Static loading:

$$y(x) = \frac{0{,}110}{1 + 14{,}522 \cdot e^{-1{,}567x}}; \qquad R^2 = 98{,}8\% \tag{3.5}$$

As for the curves fitted for the 19 mm maximum sized aggregate data, the R-squared values for Equations (3.4) and (3.5) were also near 1, indicating a reliable fit to the data. Figure 3.29 show the curves fitted for the logistic equations (logit) of the dynamic and static loading data.

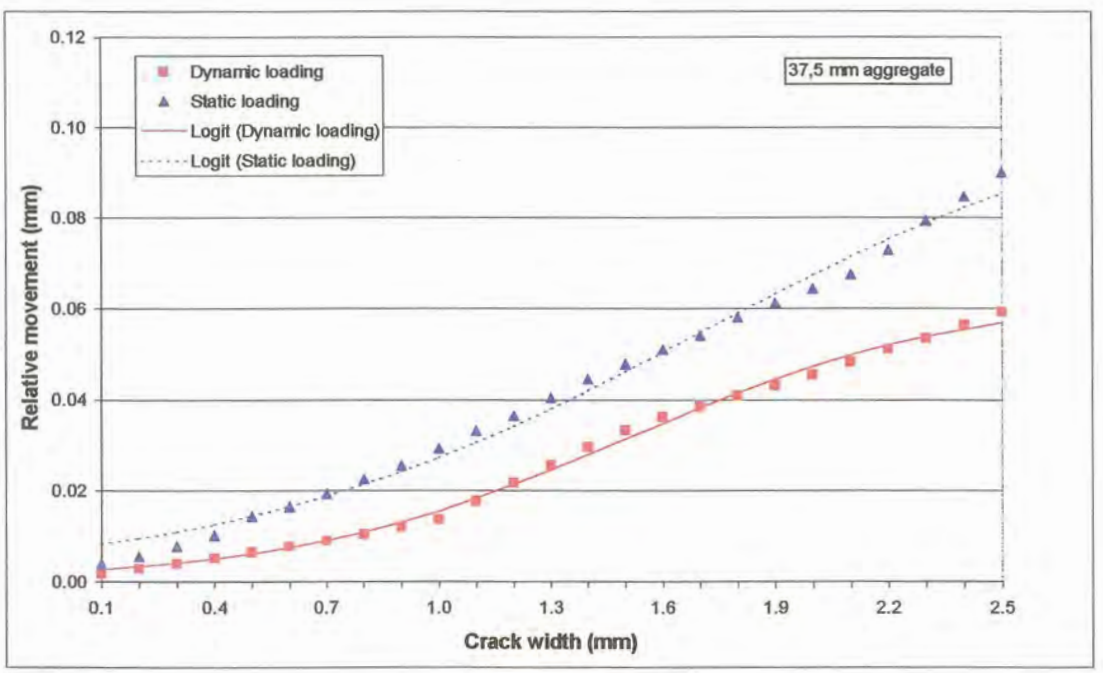

Figure 3.29: Average of RM versus crack width results for dynamic and static loading on 37,5 mm granite and dolomite aggregate

Due to the fact that the RM results for the 37,5 mm aggregate did not reach an upper asymptote at a crack width of 2,5 mm, it was decided to extend the graph to a crack width of 5,0 mm (see Figure 3.30). This was in order to establish the crack width at which the 37,5 mm aggregate tends to reach an

asymptote. From Figure 3.30 it is clear that for both dynamic and static loading of the 19 mm aggregate slabs, an almost complete S-curve was obtained with the aggregate size being small enough for the curve to reach an asymptote at approximately 2,5 mm. The crack width at which an asymptote is reached for the 37,5 mm aggregate slab seemed to be at 3,5 mm and 4,0 mm for dynamic and static loading, respectively.

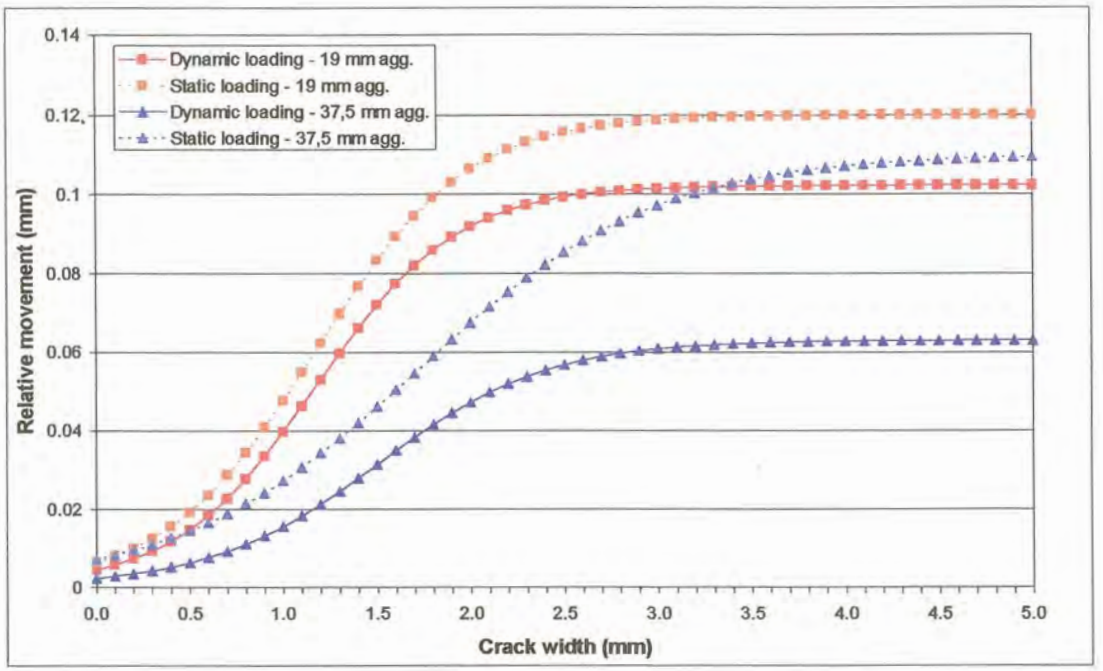

Figure 3.30: Logit function plot

It has already been mentioned that previous research projects (Colley and Humphrey, 1967; Davids et al., 1998b; Jensen, 2001) pointed out that at crack widths greater than 2,5 mm the deflection measurements tended to reach an upper asymptote and that 2,5 mm was considered as the crack width at which the subbase started to play an important role in the LTE of the concrete pavement system. The range of crack widths from 0,5 mm to 2,5 mm is considered to be the region in which aggregate interlock plays the major role in the shear load transferred across the crack. However, the results of these experiments suggest that it may be the case for the 19 mm aggregate, but not for the 37,5 mm aggregate. The fact that the asymptote for the 37,5 mm aggregate is reached at a larger crack width indicates that the region, over which aggregate interlock is still active, is also larger. This statement warrants further research, but was outside the scope of the current investigation.

The deflection and LTE results were compared with the results of a similar study conducted in the USA (Jensen, 2001). It showed that although the deflections measured were similar, the LTE obtained with the more angular crushed granite and dolomite aggregates used in South Africa, was significantly higher than the results obtained with the limestone and glacial gravel used in the USA. The 19 mm

dolomite aggregate rendered a greater LTE than a 50 mm glacial gravel blend, at a crack width of 2,5 mm.

Just as for Experiment 3, the steel frame holding the actuators was turned 90 degrees. This was in order to apply a 40 kN (the 2 actuators together) static load on the one side of the joint/crack, and compare it with the results previously obtained under 20 kN static loading.

Due to the repeated cycle of opening and closing of the two parts of the slab during initial testing, some particles were once again loosened on the crack face, which prevented closing the crack to less than 1,0 mm. Results under 40 kN load application were therefore only obtained for crack widths between 1,0 mm and 2,5 mm. Figure 3.31 show the deflection versus crack width measured on the leave slab for both 20 kN and 40 kN static loading. Although slightly higher, the deflection under 40 kN load did not differ much from the deflection under 20 kN load.

The deflection LTE in the wheelpath obtained for the 37,5 mm dolomite aggregate, subjected to both 20 kN and 40 kN static loads, is plotted on Figure 3.32. The deflection LTE lines plotted for the 20 kN and 40 kN loads were almost parallel to each other, with the 20 kN loading results slightly less than the values for the 40 kN load.

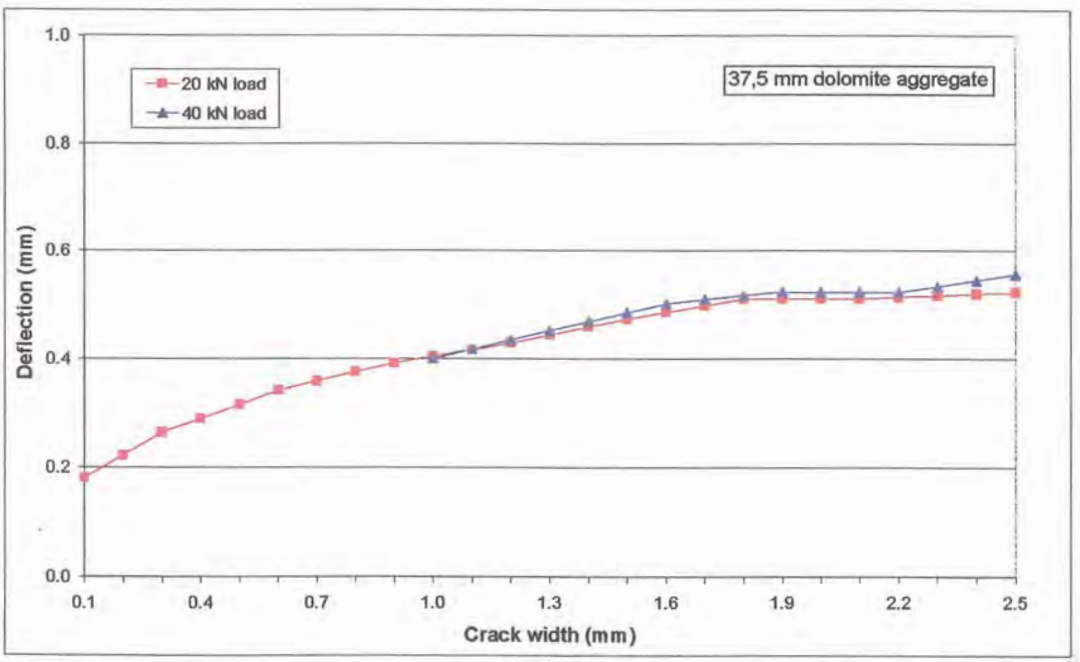

Figure 3.31: Deflection (of leave slab) versus crack width for 20 kN and 40 kN static loading (37,5 mm dolomite aggregate)

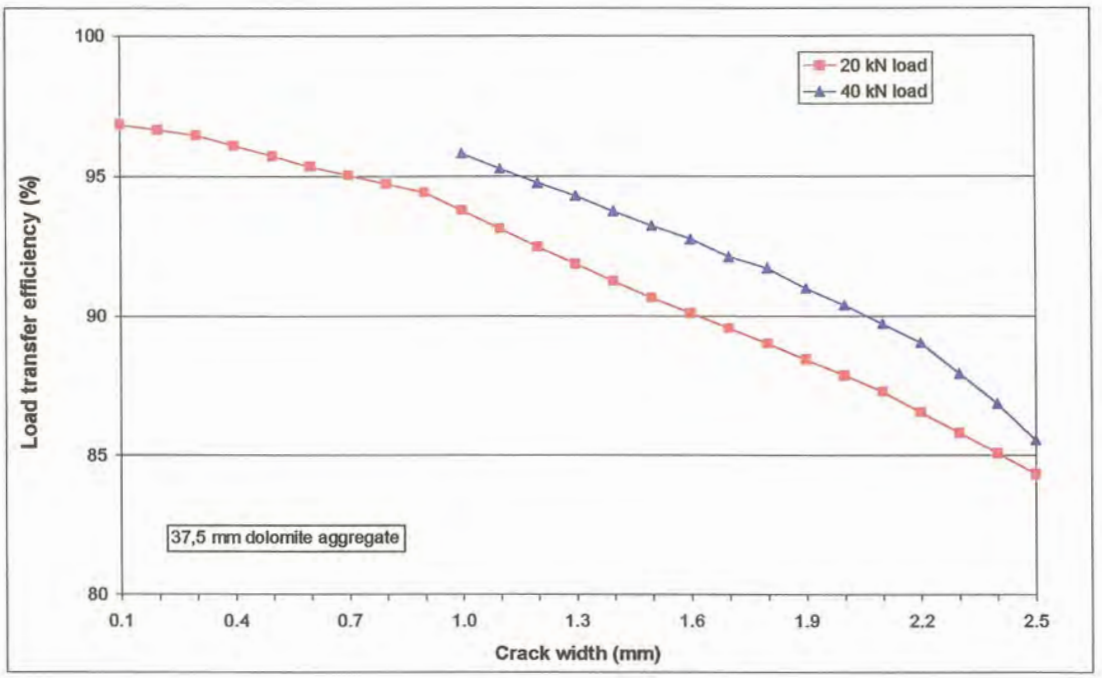

Figure 3.32: Deflection LTE – 20 kN versus 40 kN static loading (37,5 mm dolomite aggregate)

The RM measured beneath 20 kN static loading, was also compared with the RM measured beneath 40 kN static loading, and is plotted on Figure 3.33.

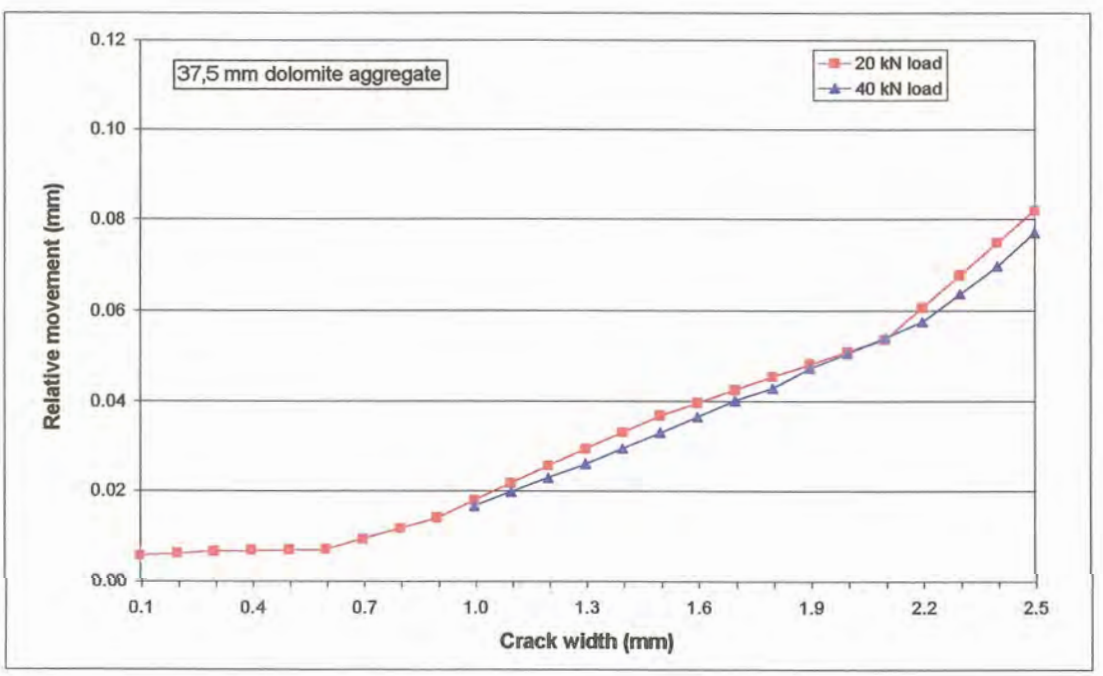

Figure 3.33: RM at joint – 20 kN versus 40 kN static loading (37,5 mm dolomite aggregate)

The RM calculated from the 20 kN loading results were higher than those calculated for the 40 kN loading. With the deflection LTE of the 40 kN load once again higher than the 20 kN load, smaller RMs for the heavier load should be expected. The scale of the vertical axis has been kept the same as that of Figure 3.24 to facilitate easier comparison between the results obtained with the 19 mm aggregate and the 37,5 mm aggregate, the RMs measured with the 37,5 mm aggregate being lower than the 19 mm aggregate.

3.3 PRE-DEFORMED PLASTIC JOINT

A fifth slab was cast using the same concrete mix design as for Experiment 1, but with a 100 micron plastic sheet at the crack position. To ensure that the concrete met the design strength requirements of 35 MPa, the 7-day cube compressive strength was determined, and a forecast made of what the 28-day results would be. This was merely for control purposes as the properties of the concrete for this specific mix design has already been determined through the tests listed in Table 3.1, and the results summarised in Appendix F.

A standard glass light bulb was used to form bubbles in the plastic, and to create an interlock effect. Figure 3.34 shows schematically what the sheet and bubbles looked like. The sheet was 600 mm wide, and 240 mm high to fit exactly into the shuttering for the slab, but with a small edge sticking out at the top (See Photo G.23).

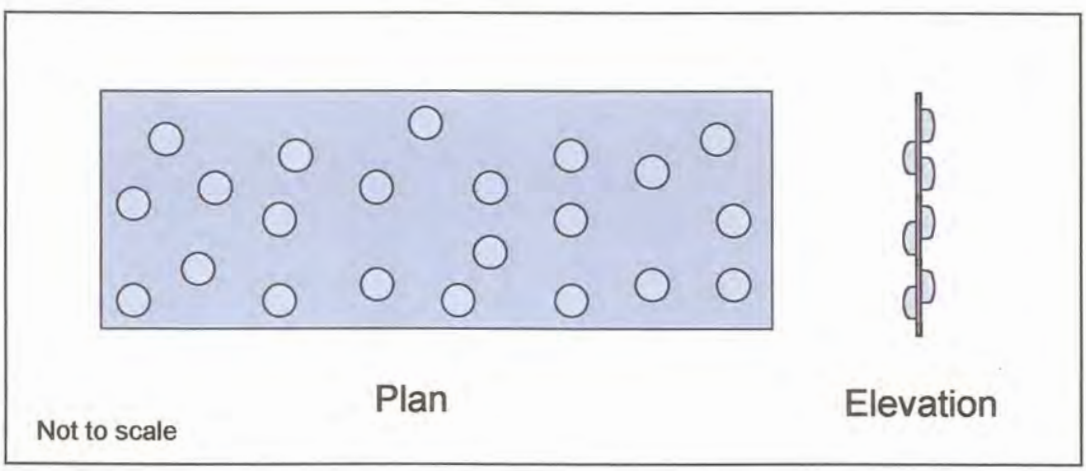

Figure 3.34: Schematic presentation of plastic joint/crack former

3.3.1 20 kN dynamic and static loading on discontinuous rubber subbase

The slab was cast on a rubber subbase with the top layer of rubber cut through. The same testing procedures as for Experiments 3 and 4 were followed for testing the characteristics of the plastic joint. The slab was subjected to three cycles of 10 minutes of dynamic loading followed by static loading at the initial crack width, where after the two sections of the slab were pulled apart and subjected to dynamic and static loading at different crack widths. The slab was pulled open up to a maximum crack width of 2,5 mm.

The data obtained was analysed in a similar fashion as the previous experimental results. The deflection versus crack width for both dynamic and static loading is shown on Figure 3.35. The deflection of the leave slab measured under dynamic loading was initially slightly higher than under static loading, due to the effect of momentum keeping the slab in a deflected position. However, as soon as the two sections of the slab were pulled apart, the smooth texture (see Photo G.24) of the surface created by the plastic sheet permitted higher deflections under static loading than under dynamic loading. The leave slab deflections increased to a maximum at a crack width of 1,2 mm under both static and dynamic loading, and then decreased again up to a crack width of 1,5 mm, where after it remained constant. For comparison purposes, the deflections measured on the approach slab were also plotted on Figure 3.35.

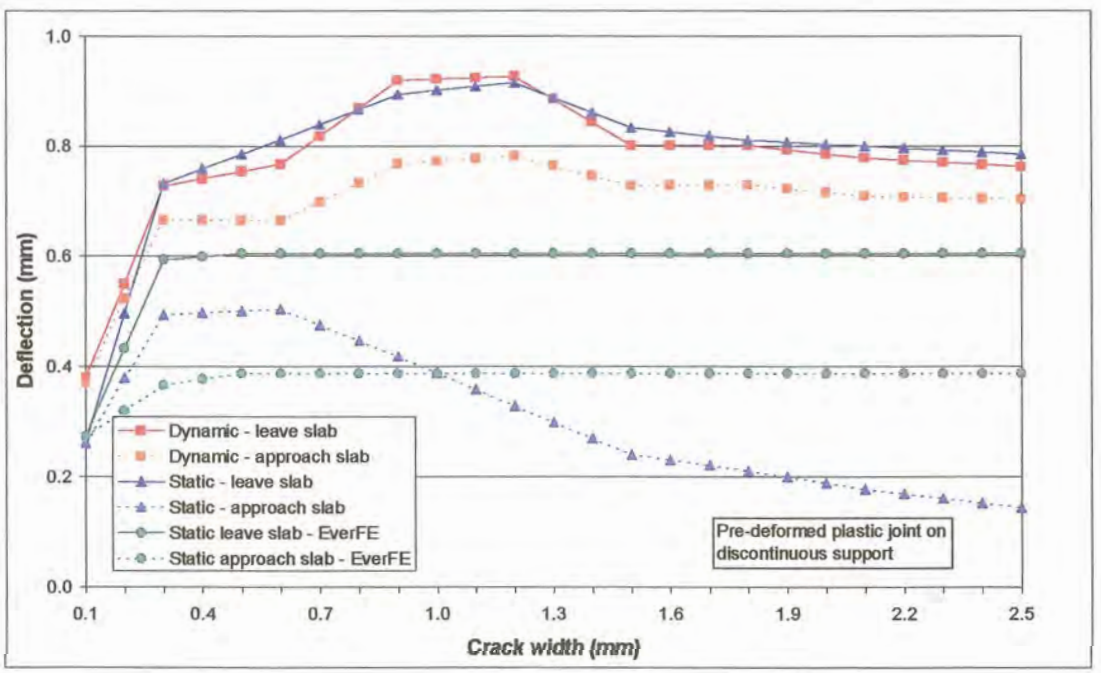

Figure 3.35: Deflection versus crack width (plastic joint on DC rubber subbase)

The deflections measured on the approach slab during both dynamic and static loading also reached a maximum, where after it decreased gradually. The increase in the difference between the deflection results with increasing crack width of the leave and approach slabs under static loading was far greater than the comparative results measured under dynamic loading.

The plastic joint was also theoretically analysed with EverFE, and the results plotted on Figure 3.35. The initial deflection calculated with EverFE for 20 kN static loading was slightly higher than the measured results. The EverFE deflection results also increased as soon as the joint/crack opened, but already levelled out after a crack width of 0,5 mm which was far sooner than the laboratory results. On the leave slab the maximum deflection calculated with EverFE was 0,60 mm, while the maximum measured varied between 0,85 mm and 0,95 mm for static and dynamic loading, respectively.

The horizontal crack displacement under both dynamic and static loading versus the crack width is given in Figures 3.36 and 3.37. For comparison purposes, the vertical axes of these two figures were once again kept the same as the previously reported horizontal crack displacement results (see also Figures 3.6, 3.11, 3.12, 3.18, 3.19, 3.26, and 3.27). The horizontal crack displacement at the top of the crack tended to be larger under dynamic loading than under static loading. At the bottom of the crack the difference in results was not so marked.

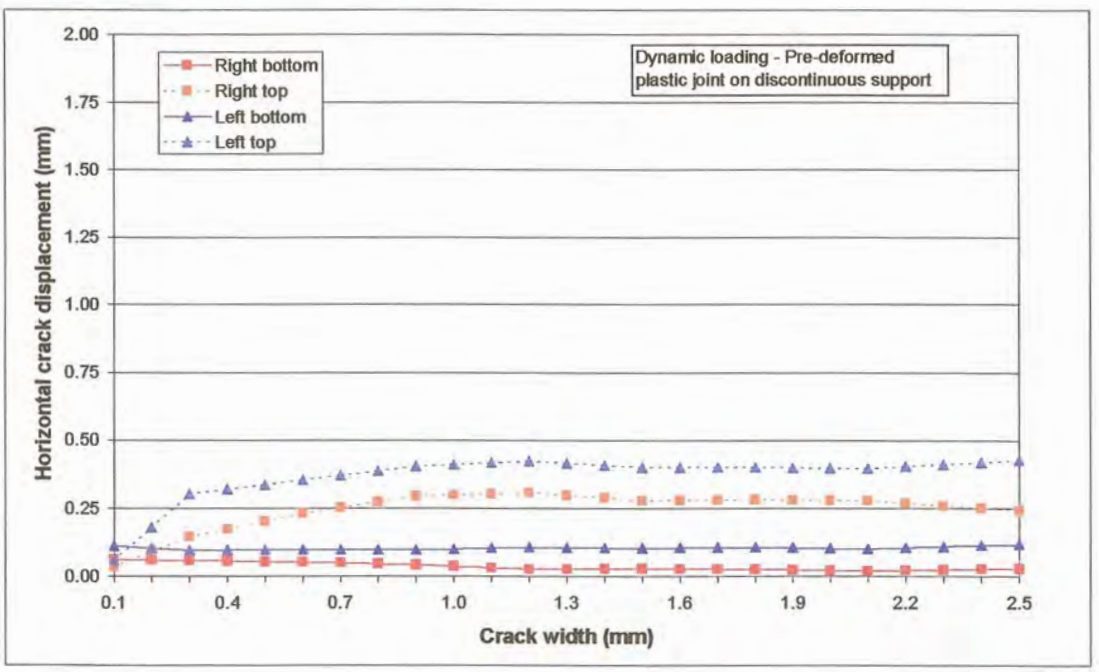

Figure 3.36: Horizontal crack displacement versus crack width under dynamic loading (plastic joint on DC rubber subbase)

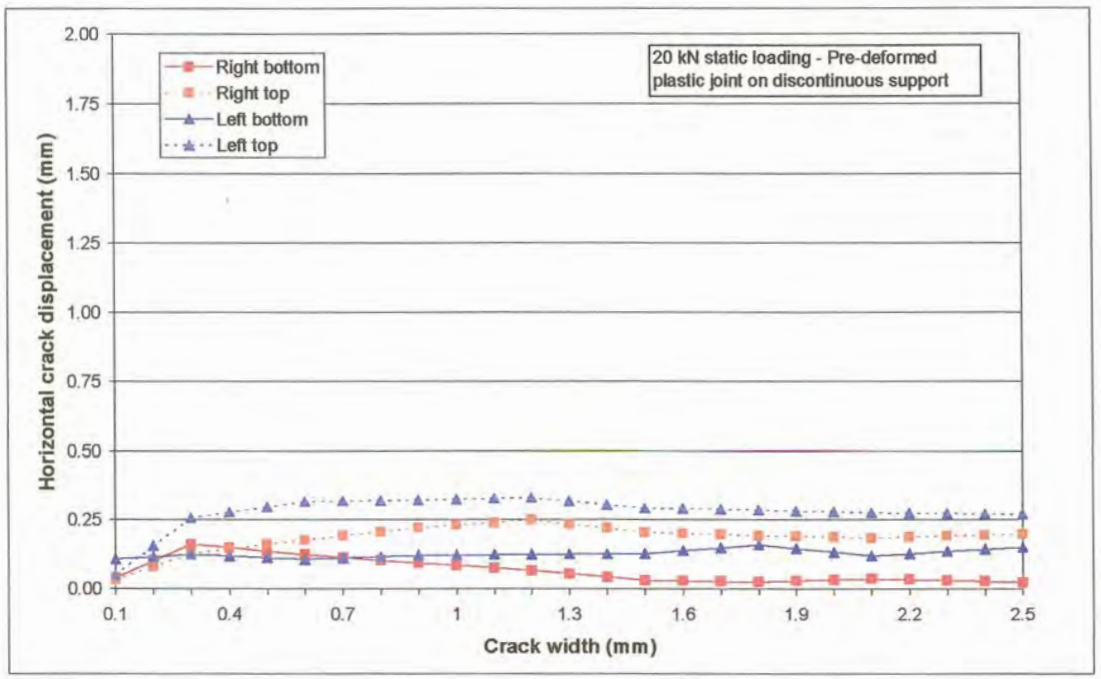

Figure 3.37: Horizontal crack displacement versus crack width under static loading (plastic joint on DC rubber subbase)

The deflection LTE for both dynamic and static loading at the initial crack width, shown on Figure 3.38, was close to 100%. The parameter controlling the performance of the slab at 0,1 mm joint/crack width was therefore the crack width itself. In this initial locked up position the two sections of the slab reacted together, with little differential horizontal or vertical movement. However, as soon as the two sections of the slab were pulled apart, the two sections slipped and slided over each other and the LTE dropped dramatically. The effect of moment and inertia in the system causing continual horizontal forces to be transferred across the joint during dynamic loading with the LTE levelling out to a value of 92% at a crack width of 2,5 mm, was remarkable during this test. A further phenomenon, is the fact that specifically under dynamic loading the LTE decreased, reached a turning point, and then increased again, where after it levelled out (the reverse of the deflection measurements).

Under static loading, on the other hand, there was a constant decrease in deflection LTE, with increasing crack width. This showed that the horizontal forces transferred across the joint were far less under static loading than what was transferred through momentum forces under dynamic loading. The EverFE results, reached a minimum turning point at a crack width of 0,3 mm, but then it also turned, increased, and levelled out similar to the dynamic loading results. Although, once again, the EverFE results levelled out at a crack width of 0,5 mm, compared to the 1,5 mm crack width where the dynamic loading results levelled out.

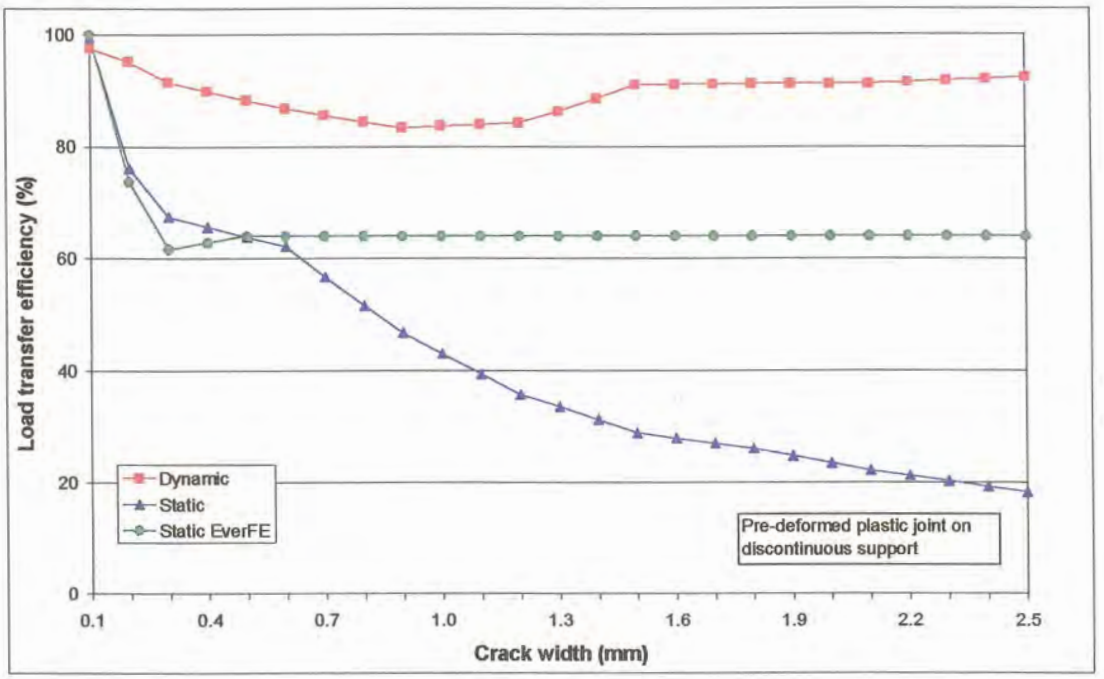

Figure 3.38: Deflection LTE versus crack width (plastic joint on DC rubber subbase)

It is the opinion of the author that the response of the plastic joint was that measured up to a crack width of 1,5 mm, and that specifically the results under dynamic loading thereafter were influenced by the subbase stiffness. This would imply that the smoother the texture of the crack face, the sooner the system will rely on the support of the subbase to transfer stresses and strains from one slab to another. This study has already indicated three such transition zones, namely: 1,5 mm for the smooth joint, 2,5 mm for the 19 mm aggregate interlock joint, and between 3,5 mm and 4,0 mm for the 37,5 mm aggregate interlock joint.

Furthermore, although it is on a micro scale, the turning point in the dynamic loading data of the plastic joint, indicate a re-orientation of the leave slab relative to the approach slab. While the two sections of the slab moved both vertically and horizontally relative to each other, the leave slab also rotated slightly. This explains why during the first slipping and sliding phase there was initially a decrease in LTE. The leave slab then rotated slightly, and found a new equilibrium point, where the graph levelled out. After this the rotation movement caused the leave slab to "lock" into a more stable position, from there the increase in LTE, where after the two sections of the slab were supported by the subbase. The smooth texture of the plastic surface inside the joint made it possible for the two sections of the slab to repeat a specific action during crack-opening testing, and thereby ensured continuity in the data.

The RMs measured at the joint/crack under dynamic and static loading, as well as the theoretical RMs determined with EverFE is shown on Figure 3.39. The RM results under dynamic loading started at zero, reached a maximum turning point, decreased again, and tended to converge to a constant value.

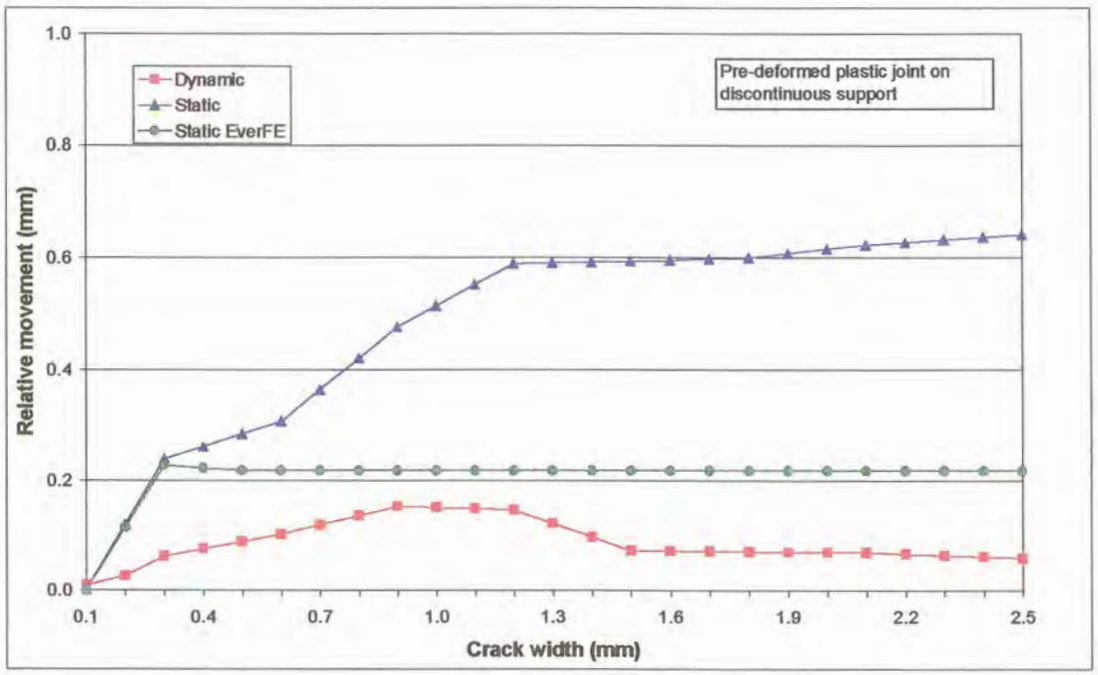

Figure 3.39: RM versus crack width (plastic joint on DC rubber subbase)

The RM results under static loading increased with increasing crack width. The theoretical EverFE results were initially approximately the same as the static loading laboratory results, but it already stabilised after a crack width of 0,3 mm.

Contrary to the RM S-curve formulas that could be derived from the aggregate interlock experiments no formula was derived from the curves drawn from the plastic joint laboratory results. After re-orientation of the leave slab relative to the approach slab, under dynamic loading, the plastic joint had a RM at a crack width of 2,5 mm about the same as the 37,5 mm maximum aggregate size results (see Figure 3.29). These results show that the actual re-orientation movement in terms of vertical slipping and horizontal sliding took place from a crack width just larger than 0,1 mm to 1,5 mm for this particular plastic joint. At crack widths larger than 1,5 mm the RM of the subbase was measured.

The RM for the plastic joint under static loading, however, gradually increased up to a value where it was 6 times higher at a crack width of 2,5 mm than the RM under static loading for the aggregate interlock joints.

3.3.2 40 kN static loading on discontinuous rubber subbase

Similar to the procedure followed during Experiments 3 and 4, the steel frame holding the actuators was turned 90 degrees, and a 40 kN static load was applied on the one side of the joint. The results

were then compared with the 20 kN static loading results already obtained. The smooth surface finish of the plastic joint face made it possible to close the crack to its original 0,1 mm width, prior to commencement of the 40 kN loading test. The deflections measured for the 20 kN and 40 kN static loading results are shown on Figure 3.40.

On the leave slab the deflection measurements under the heavier 40 kN load gradually increased with increasing crack width. The transfer of normal stresses to the approach slab could be maintained reasonably well up to a crack width of 0,6 mm, where after the deflections on the approach slab decreased with increasing crack width. This indicates a decrease in LTE with increasing crack width as can be seen from Figure 3.41. Although the heavier load initially had a lower LTE than the lighter load, it was eventually twice as effective in transferring the load across this particular type of joint.

As a final comparison for this specific test set-up, the RMs measured across the joint for 20 kN and 40 kN static loading, as well as the theoretical results determined with EverFE are plotted on Figure 3.42. The RMs under both 20 kN and 40 kN static loading seem to be still on the increase at a crack width of 2,5 mm, whereas the EverFE results already levelled out after a crack width of 0,3 mm.

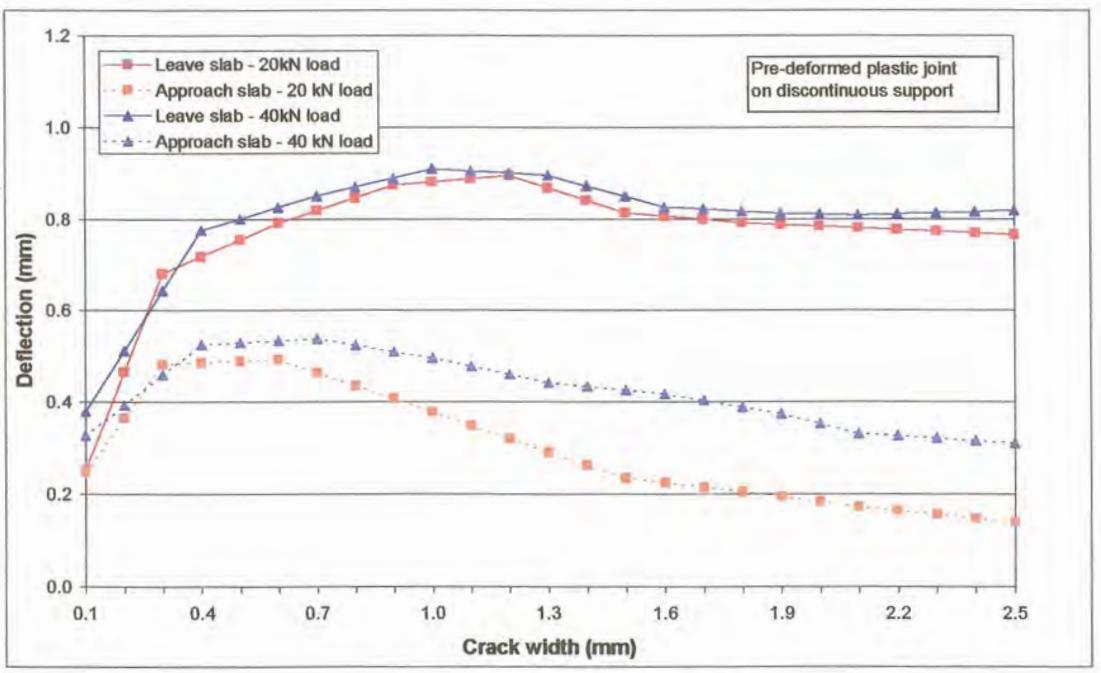

Figure 3.40: Deflection versus crack width for 20 kN and 40 kN static loading (plastic joint on DC rubber subbase)

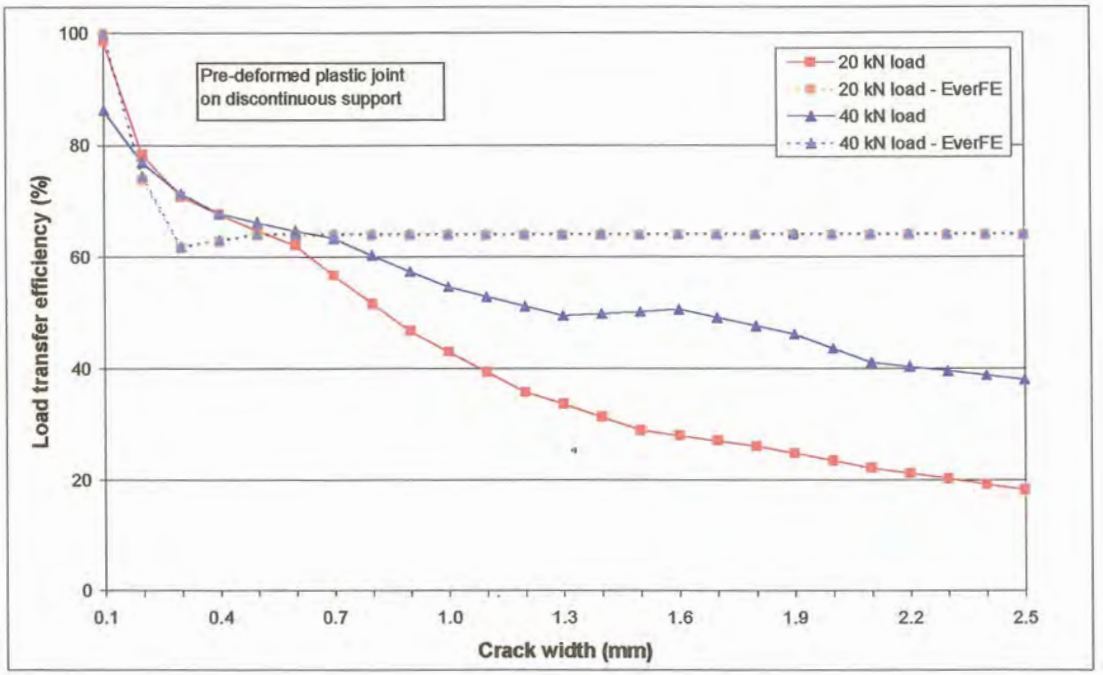

Figure 3.41: Deflection LTE versus crack width for 20 kN and 40 kN static loading (plastic joint on DC rubber subbase)

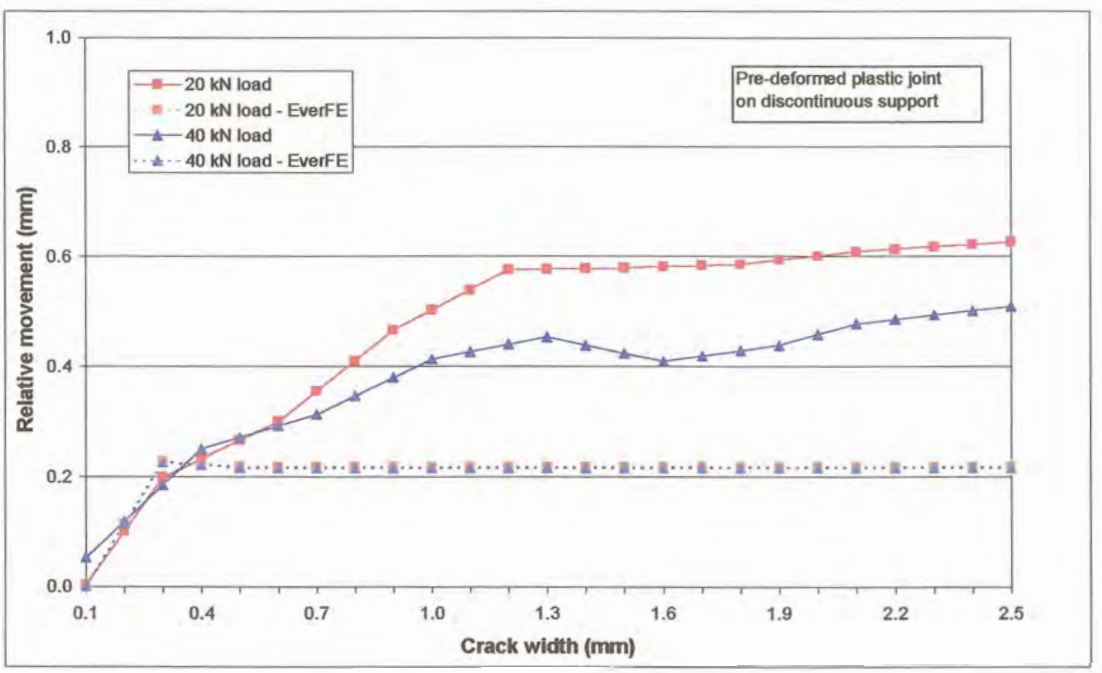

Figure 3.42: RM versus crack width for 20 kN and 40 kN static loading (plastic joint on DC rubber subbase)

3.3.3 20 kN dynamic and static loading on continuous rubber subbase

Due to the fact that the crack face formed by the plastic was relatively smooth, it was possible to lift the two sections of the slab off the top layer of rubber that was cut through, and replace it with a continuous piece of rubber, without damaging the crack face. This was in order to compare the behaviour of the concrete at the joint on a continuous (C) as well as on a discontinuous (DC) rubber subbase, and also to quantify assumptions already made in the analyses. The testing procedure with the DC rubber subbase, described in paragraphs 3.3.1 and 3.3.2, was repeated with the C rubber subbase.

The deflection versus crack width for both dynamic and static loading is shown on Figure 3.43. The deflection of the leave slab measured under dynamic loading was higher than under static loading, due to the "speed" of loading, thus due to the effect of momentum keeping the slab in a deflected position. The leave slab deflections were constantly higher than the approach slab deflections under both static and dynamic loading.

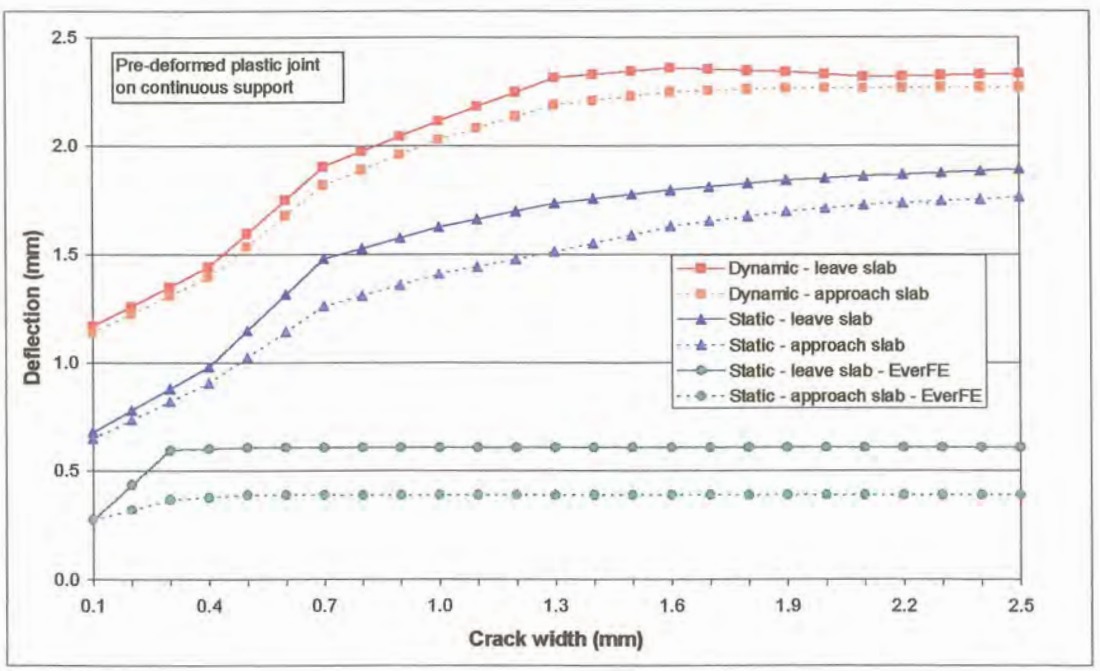

Figure 3.43: Deflection versus crack width (plastic joint on C rubber subbase)

Contrary to the marked difference between the dynamic and static loading deflection results measured on the DC rubber subbase (see Figure 3.35), the lines plotted from the deflections measured on the leave slab for both dynamic and static loading were close to parallel to the lines plotted from the deflections measured on the approach slab of the C rubber subbase. This was directly due to the greater load transfer capacity of the C rubber subbase.

The plastic joint was also theoretically analysed with EverFE, and the results plotted on Figure 3.43. The initial deflection calculated with EverFE for 20 kN static loading was only 40% of the static loading results, and only 23% of the dynamic loading results. The EverFE deflection results were consistently lower than the laboratory results.

The horizontal crack displacement under both dynamic and static loading versus the crack width is given in Figures 3.44 and 3.45. As before, the vertical axes of these two figures were kept the same as the previously reported horizontal crack displacement results. The bending through of the slab at narrow crack widths, with a reversal (between 0,7 mm and 1,3 mm crack widths), and the opening up of the top of the crack at larger crack widths was more pronounced in this instance than what was previously measured during for example Experiment 3. This could be attributed to the smooth surface of the joint/crack face. The movement at the top of the crack under dynamic loading was approximately twice the movement under static loading, which could be attributed to the effects of momentum.

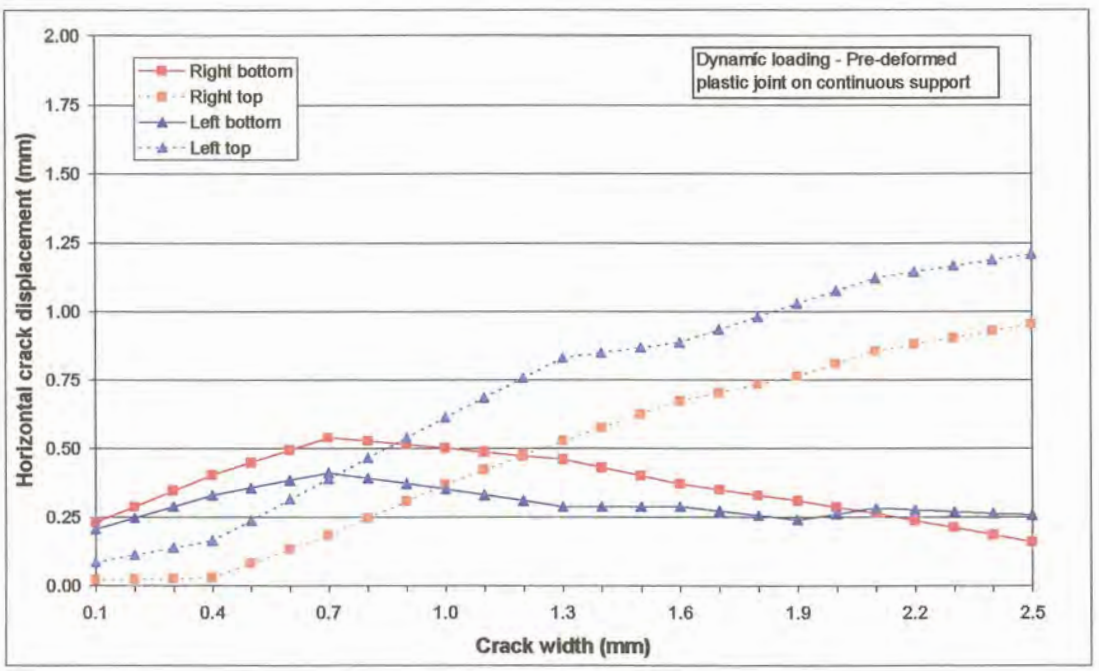

Figure 3.44: Horizontal crack displacement versus crack width under dynamic loading (plastic joint on C rubber subbase)

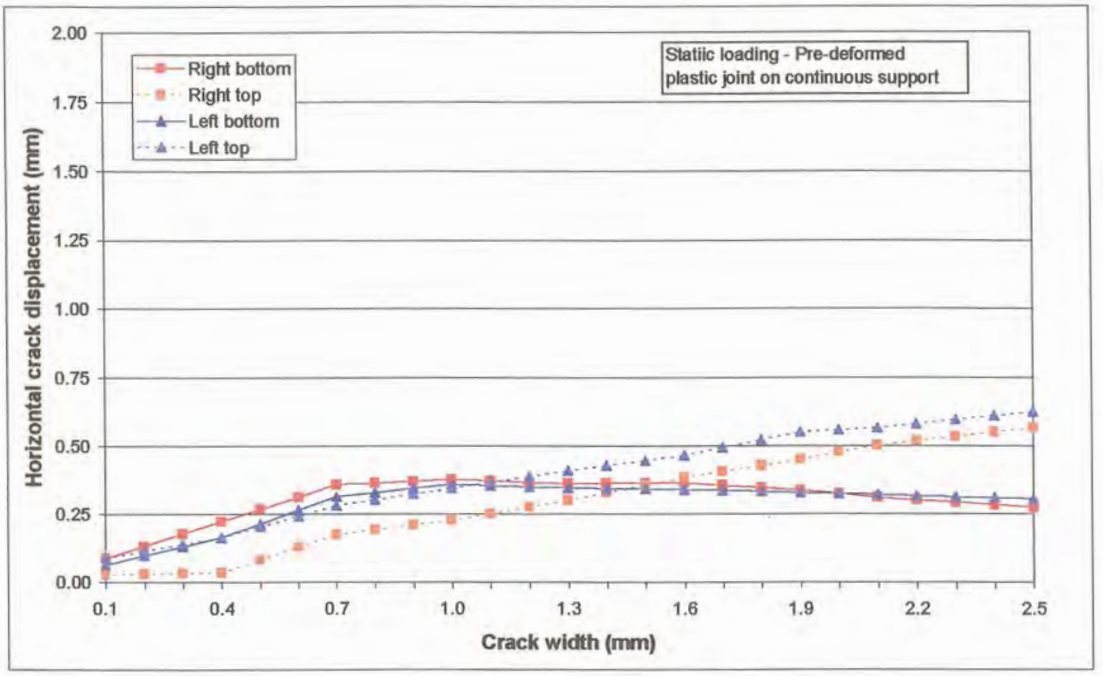

Figure 3.45: Horizontal crack displacement versus crack width under static loading (plastic joint on C rubber subbase)

The deflection LTE under dynamic loading at the initial crack width, shown on Figure 3.46, was close to 100%, with an average LTE of 96% at larger crack widths up to 2,5 mm. This was primarily due to the effect of momentum, but also due to the C rubber subbase. The LTE at a crack width of 0,1 mm under static loading was 96%. As before, applying a static load at the one side of the crack allowed sliding of the leave slab relative to the approach slab. The LTE under static loading therefore decreased, levelled out, and increased again, with the continuous subbase support ensuring greater LTE than the DC rubber subbase under similar loading conditions. From Figure 3.46 it is also obvious that the theoretical EverFE analysis results did not approximate the laboratory results.

The RMs measured between the leave slab and the approach slab under dynamic and static loading, as well as the EverFE results are shown on Figure 3.47. Both the dynamic and static loading results increased levelled out, and then decreased again, indicating a re-orientation of the leave slab relative to the approach slab. Between 0,7 mm and 1,3 mm crack widths the static loading and EverFE results were basically the same.

The most probable reason for this similarity between the laboratory and the EverFE results may lie in Walraven's (1981) aggregate interlock model incorporated in EverFE. The rounded shape of the "bubbles" in the plastic sheet can be considered as a close representation of Walraven's (1981) model where the aggregate is modelled as spherical in shape.

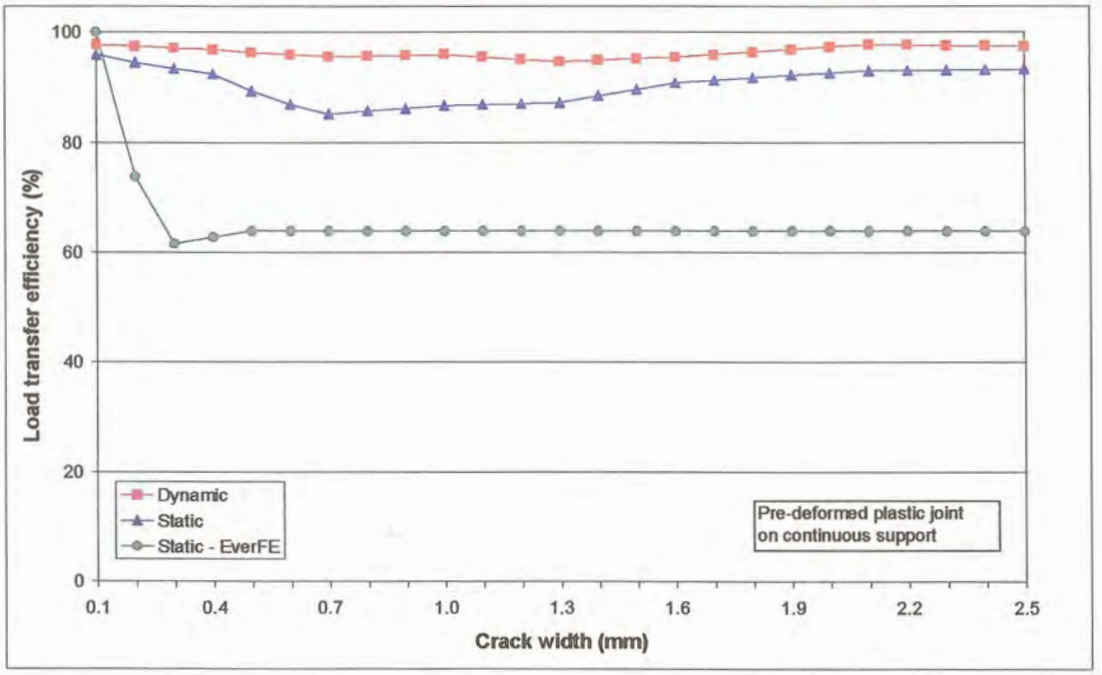

Figure 3.46: Deflection LTE versus crack width (plastic joint on C rubber subbase)

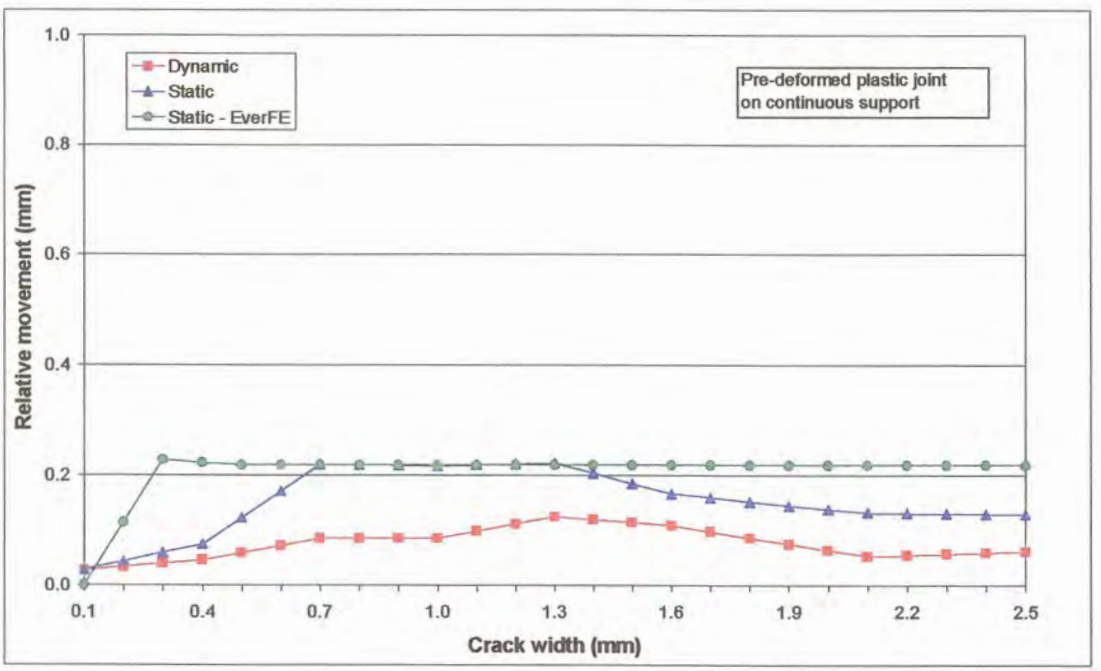

Figure 3.47: RM versus crack width (plastic joint on C rubber subbase)

3.3.4 40 kN static loading on continuous rubber subbase

As before, the steel frame holding the actuators was turned 90 degrees, and a 40 kN static load was applied on the one side of the joint. The results were then compared with the 20 kN static loading results already obtained. The deflections measured for the 20 kN and 40 kN static loading results are shown on Figure 3.48.

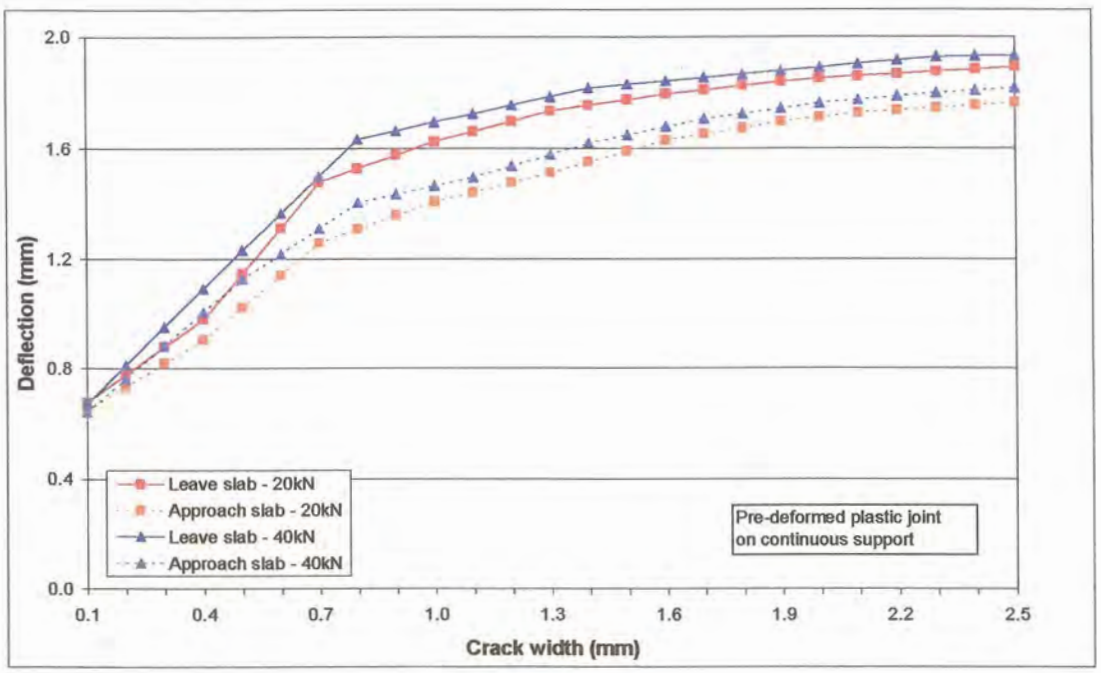

Figure 3.48: Deflection versus crack width for 20 kN and 40 kN static loading (plastic joint on C rubber subbase)

The deflection measurements under both the 20 kN and 40 kN loads gradually increased with increasing crack width. The deflections under the heavier 40 kN load were consistently higher than the deflections under the 20 kN load, with the two data sets running parallel to each other.

The deflection LTE for both the 20 kN and 40 kN static loading results are shown on Figure 3.49. The results were approximately the same, with the LTE under the heavier 40 kN load marginally higher than under the lighter 20 kN load. The theoretical results calculated with EverFE levelled out after a crack width of 0,5 mm, and eventually predicted an efficiency of only 70% of what was measured in the laboratory.

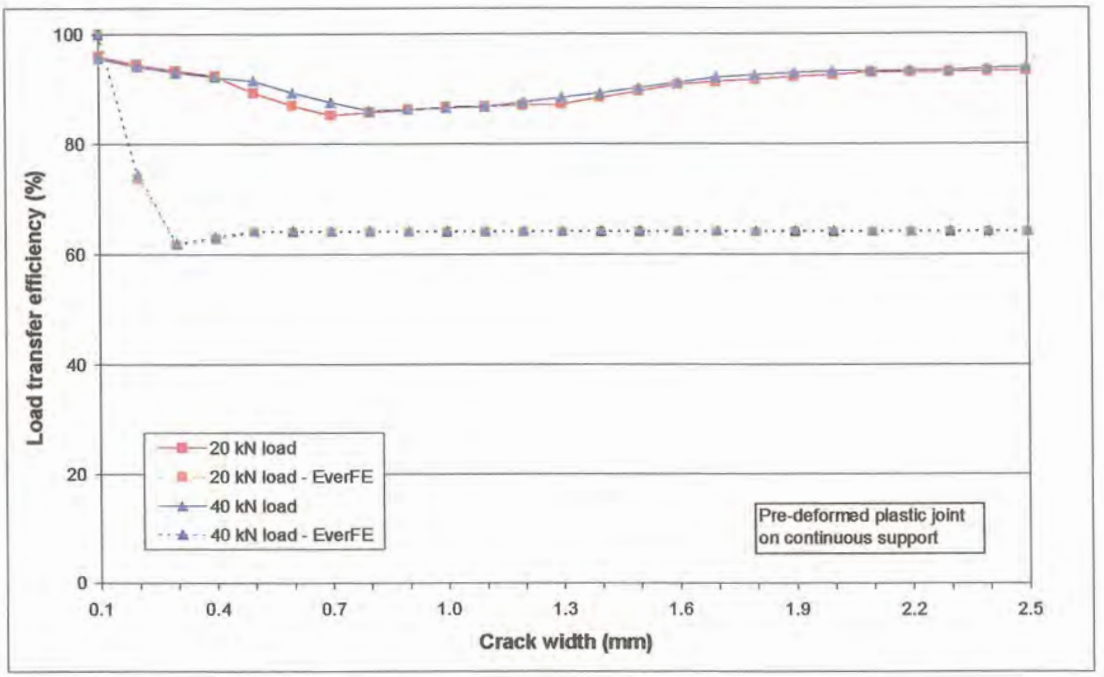

Figure 3.49: Deflection LTE versus crack width for 20 kN and 40 kN static loading (plastic joint on C rubber subbase)

The RM calculated across the joint/crack under the 40 kN load closely resembled the RM calculated under the 20 kN load (see Figure 3.50). In other words, the leave slab re-orientated itself relative to the approach slab, to the same extent under the 40 kN load as under the 20 kN load. As before, the theoretical RMs determined with EverFE are also shown on Figure 3.50. At crack widths from 0,7 mm to 1,4 mm the experimental results and the theoretical results were approximately the same.

3.3.5 20 kN dynamic and static loading - comparison between discontinuous and continuous rubber subbase

By subjecting the same concrete slab to the same set of tests, but with different subbase types, it was possible to quantify the effect of the subbase support on deflection, LTE, and RM at the joint/crack.

Figure 3.51 illustrates the fact that the continuous, rubber subbase accommodated greater deflections at the same crack width than the DC rubber subbase. This was already noticed during analysis of the data obtained from the first four experiments. The deflection results of Experiments 1 and 2 (see Figures 3.5 and 3.13) on the C rubber subbase were approximately 3 times higher than the comparative results of Experiments 3 and 4 (see Figures 3.17 and 3.25).

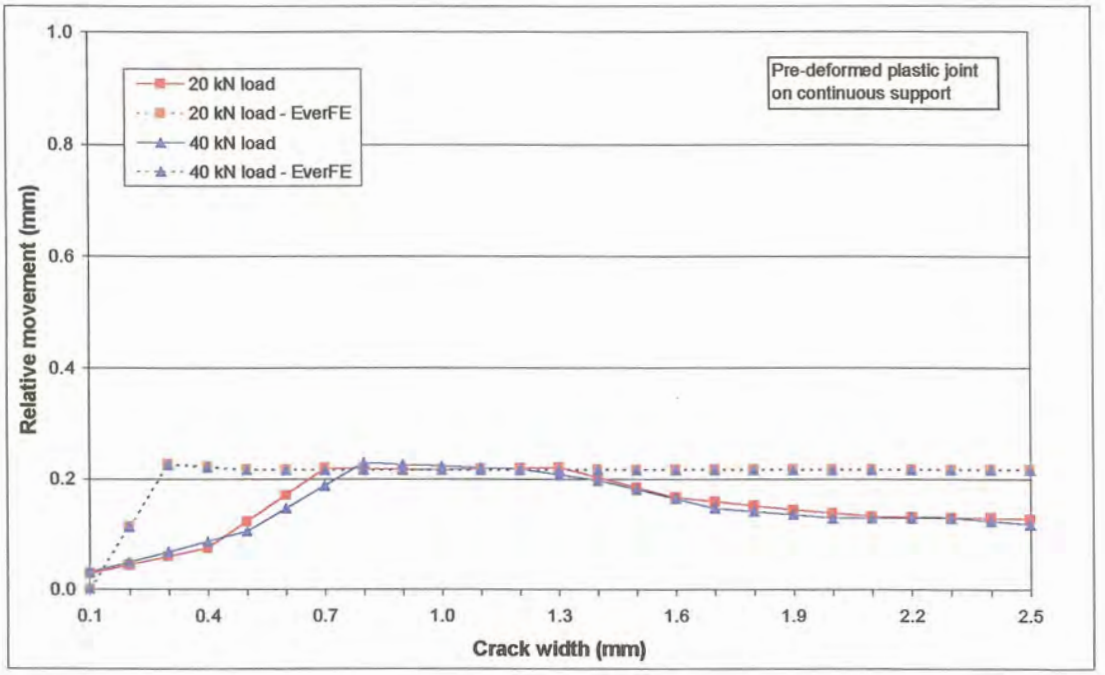

Figure 3.50: RM versus crack width for 20 kN and 40 kN static loading (plastic joint on C rubber subbase)

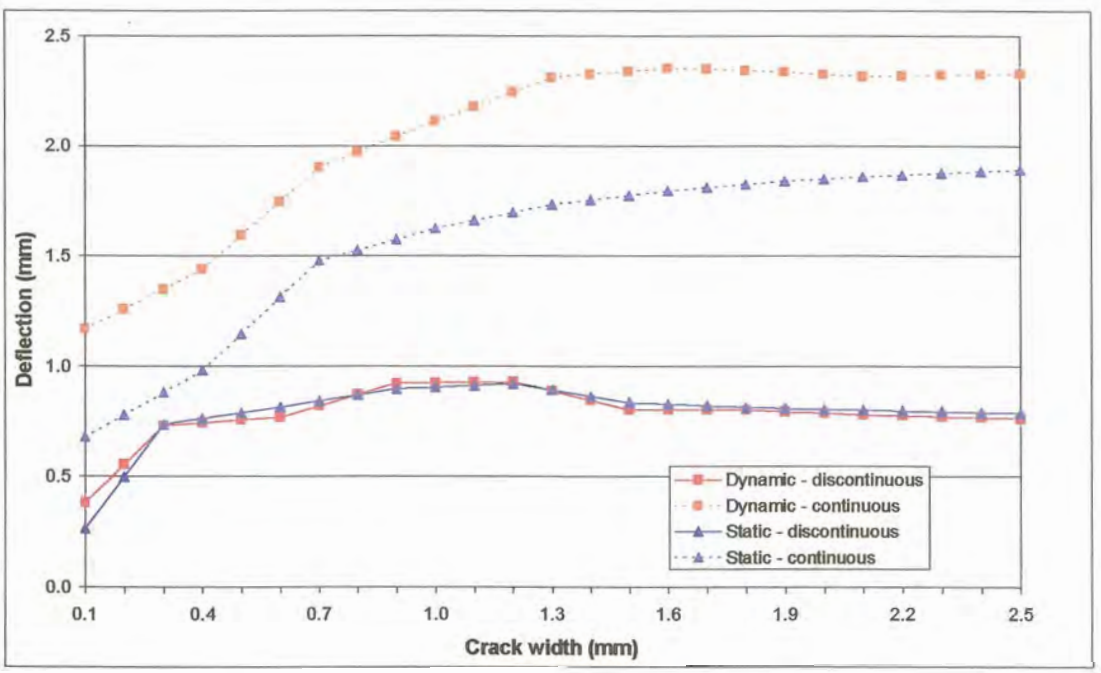

Figure 3.51: Deflection versus crack width – comparison between DC and C rubber subbase (plastic joint)

Despite the higher deflections measured with the C rubber subbase, than with the DC rubber subbase, the LTE was also higher on the C rubber subbase than on the DC rubber subbase. This is illustrated in Figure 3.52.

The C rubber subbase therefore assisted the concrete to have a greater capacity to transfer both horizontal and vertical stresses and strains across the joint/crack. Under dynamic loading the effects of momentum further increased this capacity with the LTE under dynamic loading higher than under static loading in all instances.

The LTE calculated on the DC rubber subbase under dynamic loading was similar to the static loading results from the C rubber subbase. The DC rubber subbase therefore inhibited the transfer of stresses and strains across the joint/crack. This was obvious from the constant decrease in LTE with increasing crack width under static loading. But, on the other hand, the effect of momentum aided the transfer of load across the joint, and therefore the similarity between the above mentioned results.

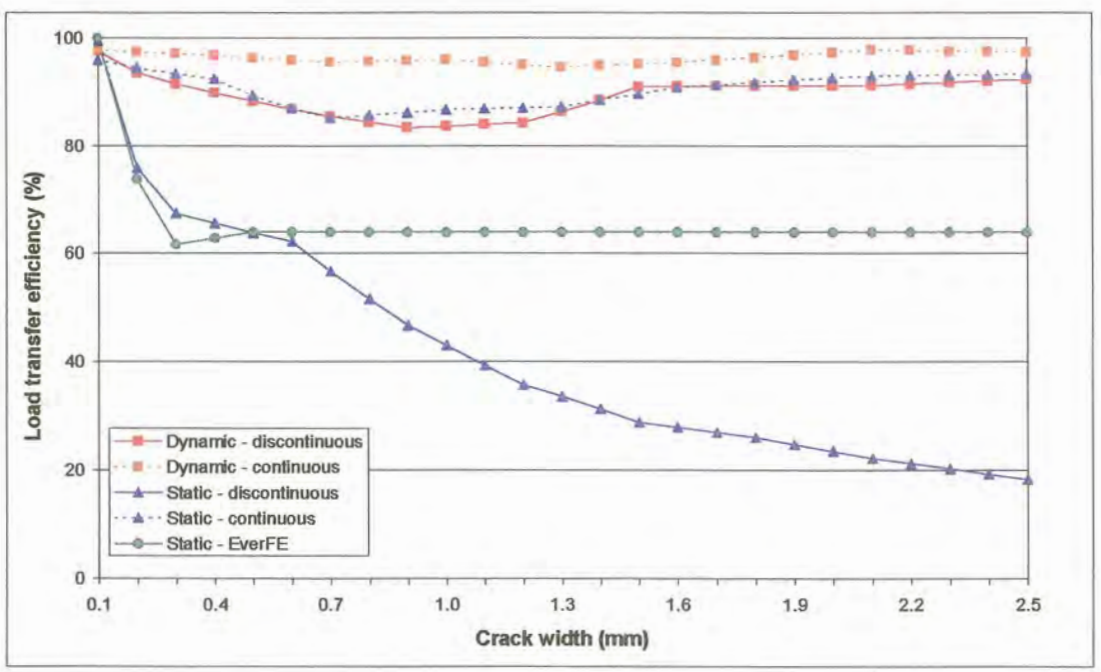

Figure 3.52: Deflection LTE versus crack width – comparison between DC and C rubber subbase (plastic joint)

When comparing the RMs calculated from the deflection results, the dynamic loading results for both subbases tested were remarkably close, as shown on Figure 3.53.

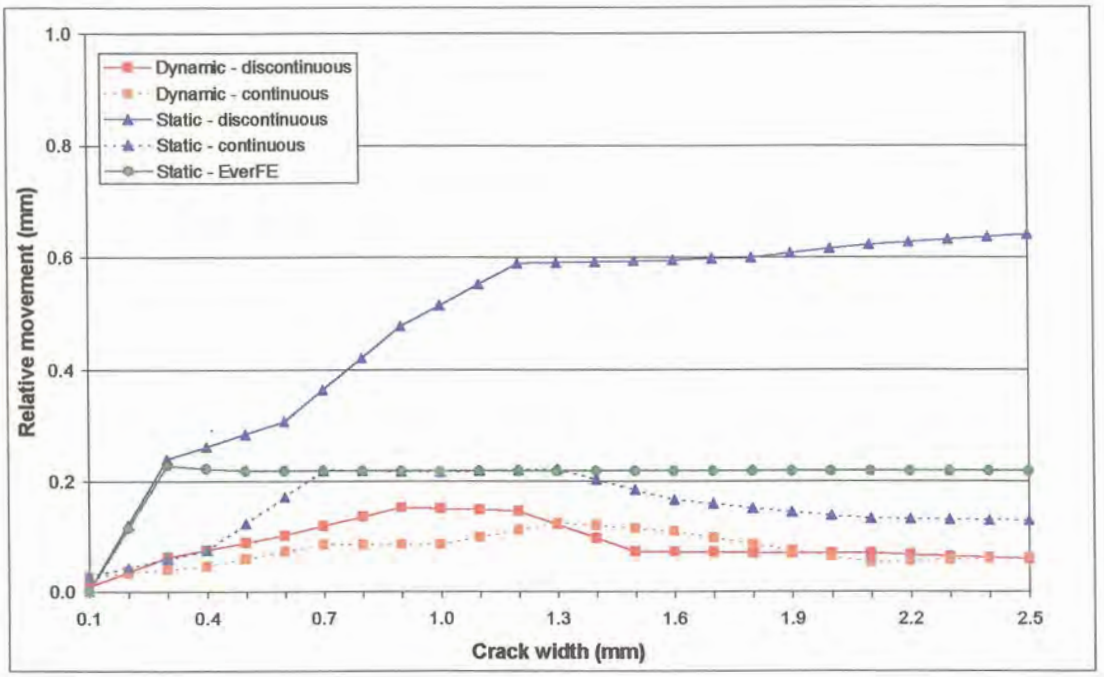

Figure 3.53: RM versus crack width – comparison between DC and C rubber subbase (plastic joint)

Bearing in mind that the smooth plastic joint surface had little interlock capacity, it could be expected that the RMs under static loading would not be similar. Just as the continuous subbase had a greater LTE under static loading than the discontinuous subbase, it therefore had the ability to reduce RM between the two sections of the slab, thereby yielding smaller RMs for the continuous subbase than for the discontinuous subbase.

An important point that needs to be stressed here, is that due to the smooth surface texture of the plastic joint, the static loading results were different, but during analysis of the results obtained for Experiments 1 to 4, the static loading results for the same maximum aggregate size concrete mixes were similar, and could therefore be combined. This could be attributed to the coarseness of the aggregate interlock crack faces. This factor was quantified by conducting volumetric surface texture tests on all relevant samples, as described in Appendix F.

3.3.6 20 kN and 40 kN static loading - comparison between discontinuous and continuous rubber subbase

The application of a 40 kN static load on the one side of the crack has been discussed in paragraphs 3.3.2 and 3.3.4. To facilitate an easier comparison, the data from these experiments has also been combined into single graphs. Figure 3.54 present the deflections measured for the leave slab on both the DC and the C rubber subbases, for 20 kN and 40 kN static loading.

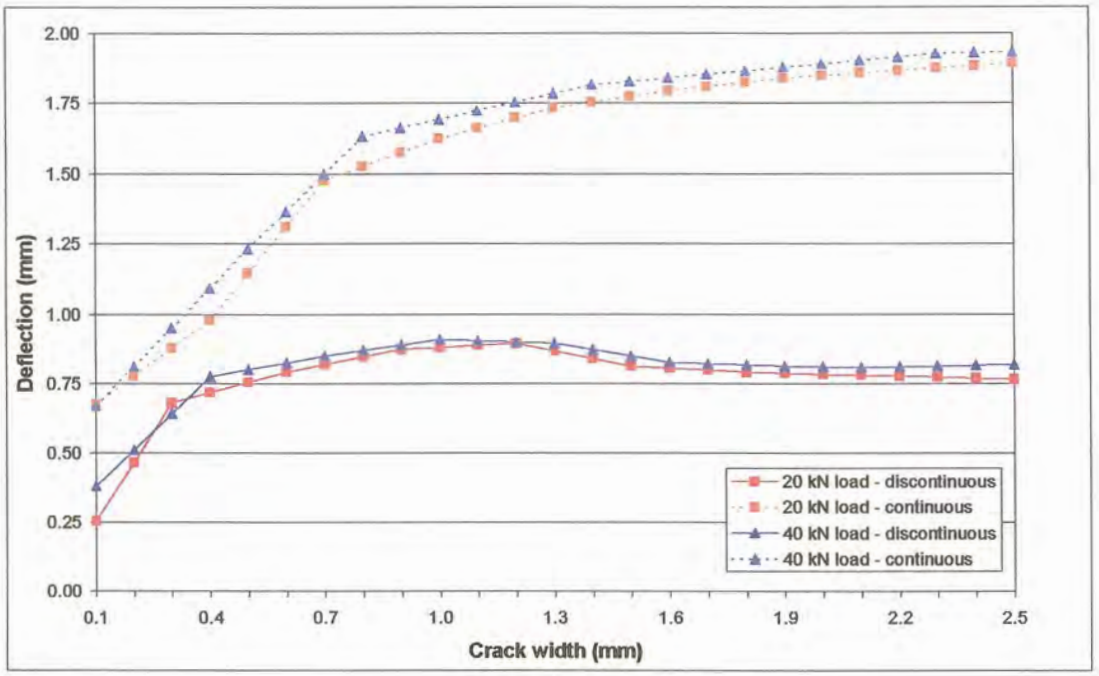

Figure 3.54: Deflection versus crack width – comparison between 20 kN and 40 kN static loading on DC and C rubber subbases (plastic joint)

Although the 20 kN and 40 kN loading results on the distinguishable subbases were similar, the deflections on the C subbase were approximately 2,5 times that of the DC subbase. As before, the C rubber subbase assisted the concrete to have a greater capacity to transfer both horizontal and vertical stresses and strains across the crack.

The combined LTE data is presented in Figure 3.55. As indicated before, the C rubber subbase, although it allowed higher deflections, had a LTE of 5 times that of the DC rubber subbase with the 20 kN static loading and 2,5 times that of the DC rubber subbase for 40 kN loading. As mentioned before, although the heavier load on the DC rubber subbase initially had a lower LTE than the lighter load, it was eventually twice as effective in transferring the load across this particular type of crack and the only case where doubling the load, doubled the LTE at a crack width of 2,5 mm. On the other hand, the LTE on the C rubber subbase for both 20 kN and 40 kN loading was very similar. The implication of this is that the smoother the crack face, combined with a crack reflecting into the subbase, the greater the effect or influence of the magnitude of the load. The opposite has however also been shown here and that is that although the crack face was smooth, the C (sound) rubber subbase supported the two parts of the slab to such an extent that the magnitude of the load did not have a large influence. The LTE calculated with EverFE did not resemble either of the two subbase conditions tested.

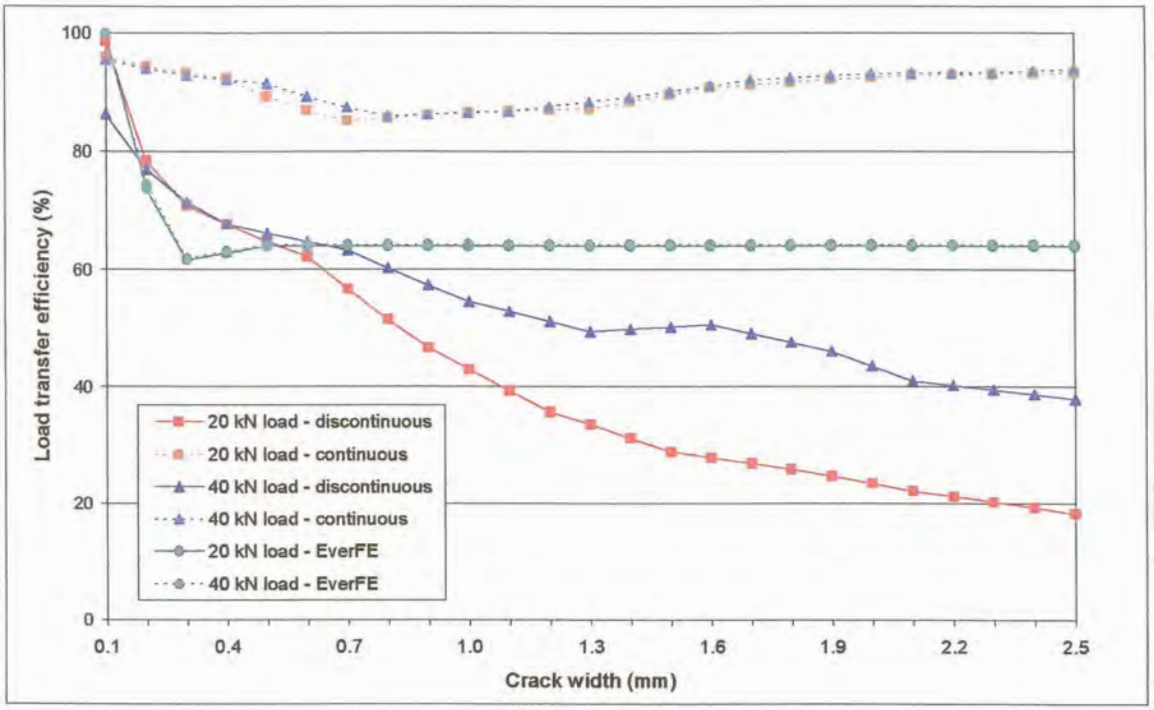

Figure 3.55: Deflection LTE versus crack width - comparison between 20 kN and 40 kN static loading on DC and C rubber subbases (plastic joint)

The RM data is presented in Figure 3.56. On the DC rubber subbase, the RMs under both 20 kN and 40 kN static loading seem to be still on the increase at a crack width of 2,5 mm, whereas the EverFE results already levelled out after a crack width of 0,3 mm. The RM calculated across the joint/crack on the C rubber subbase under the 40 kN load closely resembled the RM calculated under the 20 kN load (see Figure 3.56). In other words, the leave slab re-orientated itself relative to the approach slab, to the same extent under the 40 kN load as under the 20 kN load. The theoretical RMs determined with EverFE are also shown on Figure 3.56. At crack widths from 0,7 mm to 1,4 mm the experimental results and the theoretical results were approximately the same. The rounded shape of the "bubbles" in the plastic sheet can be considered as a closer representation of Walraven's (1981) model where the aggregate is modelled as spherical in shape and therefore the similarity between the laboratory and EverFE results over this range of crack widths.

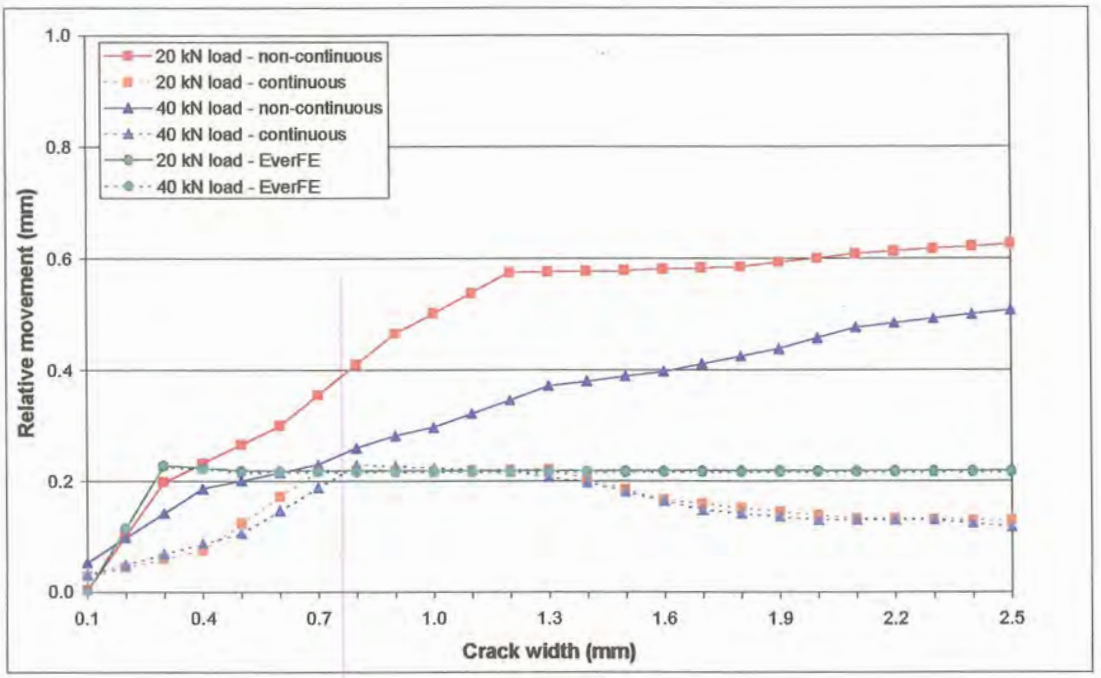

Figure 3.56: RM versus crack width - comparison between 20 kN and 40 kN static loading on DC and C rubber subbases (plastic joint)

3.4 FIELD INVESTIGATIONS

3.4.1 Introduction

Four existing southern African jointed concrete pavements (JCPs) were chosen at random for comparison of field investigation results. These pavements varied in condition from a pavement in a terminally failed condition, in service for more than 30 years, to a pavement in a good condition of which the concrete overlay has been in service for approximately 14 years. Three of the pavements had concrete shoulders, and one had asphalt shoulders. Each of the concrete pavement sections is described in terms of existing pavement design, field investigations conducted, and a structural evaluation with remaining life (RM) predictions. The data presented here has been published in design reports and were analysed by different individuals through various methods and techniques to calculate the RM for each.

The four concrete pavement sections will be discussed under the following headings:

a) Road Section 1 - concrete pavement with concrete shoulders, situated in a moderate climatic region, in a terminal condition

b) Road Section 2 - concrete overlay (on asphalt) with concrete shoulders, situated in a wet climatic region, in a good condition

c) Road Section 3 - concrete pavement with asphalt shoulders, situated in a wet to moderate climatic region, in a fair condition

d) Road Section 4 - concrete pavement with concrete shoulders, situated in a moderate climatic region, in a good condition

In the context of this study, a pavement in a terminal condition will be expected to show extensive slab cracking, both transverse and longitudinal cracks, with edge breaks, and large relative movements (RMs) with low load transfer efficiency (LTE) at joints. The effect of this will be that the pavement will have a poor riding quality. On the other hand, a pavement in a good condition typically has a sound appearance with little slab cracking and edge breaks, and low deflections with high LTE at joints. The latter pavement will also have a good riding quality.

The following paragraphs present a summary of the data from four in-service pavements. In the following chapter (Chapter 4), the data is compared by analysing the RMs measured, calculating the joint shear stiffness from the LTE results, and conducting CncRisk analyses.

3.4.2 Road Section 1

3.4.2.1 Existing pavement design

Road Section 1 is situated in a moderate climatic region (5 > N > 2; Weinert, 1964) in the South African province of Mpumalanga. Mechanical weathering could therefore be expected as the main mode of deterioration of the in situ and pavement materials under the prevailing environmental conditions. The design of the pavement, originally constructed in 1972, is given in Table 3.3.

Table 3.3: Existing pavement of Road Section 1

Layer	Thickness (mm)	Description	CBR values	
			Range	Average
Surfacing	200	Jointed Portland cement concrete	-	-
Subbase	150	Cement stabilised natural gravel	19 – 265	95
Selected	150	Natural gravel	10 – 160	30
Subgrade or fill	Varying	In situ or natural gravel	2 – 400	85

Since construction the pavement has undergone two cycles of heavy rehabilitation involving extensive crack and joint sealing and repair work to the concrete surfacing. The first cycle was during 1985, and the second during 1999. In total approximately 10% of the concrete blocks were replaced during these rehabilitation actions.

3.4.2.2 Field investigations

Field investigations consisted of visual surveys to determine typical distress types. Falling Weight Deflectometer (FWD) testing was conducted to obtain maximum deflection, deflection bowl characteristics, and RM at joints. Elastic modulus values for the layers beneath the concrete were derived from Dynamic Cone Penetrometer (DCP) testing, and cores drilled in the concrete pavement provided slab thickness, the depth of the void between the slab and subbase, and the condition of the surfacing of the subbase. Cores were also tested in the laboratory to obtain the compressive strength of the concrete.

Measured in terms of 5 block units (= 22,5 m road length) of distress, the extent of structural cracks were 32%, pumping 1,2%, and faulting (> 4 mm) 8,4%. The extent of small, medium and large repairs were 32,3%, 12,6%, and 3,5%, respectively.

The average mid-slab deflection under 40 kN load was 0,114 mm and values ranged from 0,071 to 0,247 mm for the eastbound lane. For the westbound lane the average value was 0,116 mm with a range from 0,074 to 0,189 mm. The average RMs at joints on the eastbound lane were 0,10 mm, compared to 0,07 mm for the westbound lane. The eastbound lane also had a higher average joint deflection of 0,27 mm, versus 0,22 mm for the westbound lane.

Compressive strengths obtained from the cores drilled at positions between joints where the concrete was considered to be undamaged ranged from 32,5 MPa to 40,5 MPa with an average of 37,0 MPa. Slab thicknesses determined from cores drilled at joints ranged from 185 mm to 215 mm with an average of 198,3 mm.

Measurements of voids between the concrete slab and the subbase ranged from 0 mm to 20 mm. No voids were found where cores were drilled in the middle of slabs between joints, but voids occurred at joints where the voids were generally bigger on the approach side of the joint as compared to the leave side. The actual crack widths could not be determined on site due to the failed condition of the concrete at the joints, and the fact that sound cores could not be retrieved.

Observations made during field investigations included the following:

a) Signs of pumping were only observed where the subbase appeared to be in a sound, un-cracked condition, due to abrasion of the subbase material
b) Deflections were significantly higher where voids could be detected beneath the slab. This is logical, as the bigger the void, the larger the space that can be taken up during deflection testing.
c) Muddy material could be detected on top of the subbase under the leave slab, whereas the surface of the subbase under the approach slab was clean where faulting was found. This can

be attributed to the mechanism of pumping, and the formation of voids beneath the approach slabs in the concrete overlay. When a vehicle approaches a transverse joint in the concrete pavement moisture and loose particles inside and beneath the joint position get pushed forward, and accumulate beneath the approach slab. As soon as the vehicle then moves across the joint, the loose particles and moisture are ejected back in the direction opposite to the direction of vehicle movement, as well as up through the joint. This results in a gap beneath the approach slab, and the build-up of muddy material beneath the leave slab, thereby the faulting (Barksdale, 1991).

d) Faulting occurred more frequently where traffic moved at lower speeds against steep uphill gradients. The mechanism that creates faulting is similar to that of pumping, but in this instance the material projected back from the approach slab during dynamic loading, gets compacted beneath the leave slab, causing the leave slab to lift up relative to the approach slab.

e) Faulting also occurred where no gaps existed between subbase and slab. In these cases, a crack also occurred in the subbase directly below the joint as the layer below the subbase deformed due to a low elastic modulus (measured with the DCP).

f) The crack/joint faces were in a deteriorated condition with abrasion of both the concrete and the aggregate due to repeated RMs at the joint face. Stress cracking through the aggregate as well as rounding of the aggregate through this abrasion also occurred. The fact that stress cracking occurred through the aggregate indicates that although individual aggregates may have had weak planes, the crack formed in mature, hardened concrete where the cement paste has already hardened around the aggregate. In the present study, the crack was forced to form within 24 hours after casting the slabs, to make certain that cracking took place around aggregate particles and thereby ensuring the coarsest possible crack face. The rounding of the aggregates through abrasion could be attributed to the fact that Road Section 1 has already been exposed to environmental influences and traffic loading for more than 30 years and that it has taken far more than the 2 million load cycles initially applied in the laboratory.

3.4.2.3 Structural evaluation and remaining life

Mechanistic models of the pavement were developed from field data and testing conducted at selected positions, representing the conditions encountered along the entire road section. Table 3.4 shows models from these typical positions where the pavement was investigated in detail.

Table 3.4: Detailed modelling of the pavement structure

Position		Westbound (km)			Eastbound (km)		
		1,59	**38,6**	**33,8**	**35,1**	**38,4**	**5,2**
Slab thickness (mm)*		215/213	200/202	200/197	187/200	190/190	185/195
Back-calculated Elastic modulus (MPa)	Slab	35 000	37 000	37 000	30 000	37 000	31 000
	Subbase	1700/750	500/450	350/120	200/70	700/700	100/400
	Selected	160	75	125	80	60	90
	Subgrade	300	75	250	95	80	30
40 kN Deflection (mm)*		0,12/0,29	0,18/0,28	0,19/0,33	0,27/0,38	0,21/0,26	0,27/0,34
RM (mm)*		-/0,26	-/0,07	-/0,18	-/0,17	-/0,11	-/0,08
LTE (%)		10	75	45	55	58	76
Void length (m)*		-/3,0	-/2,0	-/3,0	-/1,5	1,5/2,5	2,0/2,0
Load transfer constant*		0,2/0,6	0,2/0,4	0,2/0,6	0,2/0,4	0,2/0,3	0,2/0,3
Condition		Pumping	5 mm fault	Fault/crack	5 mm fault	10 mm fault	Crack
*Note: Values given are for mid-slab (internal) and at the joint itself							

Although the average deflections at joints were 0,26 mm to 0,38 mm, localised high deflection values of 0,83 mm and 0,96 mm were also recorded during the deflection survey. Deflections were measured every 200 m along the length of the road section.

It is interesting to note that the subbase stiffness at joints was generally lower than at mid-slab positions. Assuming an initial subbase stiffness modulus of 1 500 MPa (Theyse et al., 1996), the values in Table 3.4 indicate a loss of some 44% in subbase stiffness with time. This was probably due to the ingress of water at the joints.

Using the data from typical sections along Road Section 1 as summarised in Table 3.4, the average deflection (0,25 mm) and movement at joints (0,10 mm) were simulated in the original software (containing Equation (2.12)) developed for the new mechanistic concrete pavement design method (Strauss et al., 2001). It was found that the average RM was between 1,0 and 1,5 million standard 80 kN (E80) axles. This implied that after a further 1,5 million E80's, the risk of failure was 50%. The load transfer constant for the average condition was 0,49 and the length of the void between slab and subbase 1,5 m. A load transfer constant of 0,18 is used for internal loading, 0,6 for a free moving joint (edge loading), and normally a value of 0,35 is applicable for an un-dowelled joint which has been exposed to the environment and traffic for some 15 years.

The reasons for the pavement having been in such a poor condition could be summarised as follows:

a) The pavement was designed for an expected 6 million E80's. At the time of investigation the axle loading was 858 E80's/day westbound and 677 E80's/day eastbound. Projected over a period of 4 years, assuming a traffic growth rate of 3%, this meant 1,3 million E80's westbound and 1,1 million E80's eastbound. An average RM of 1,5 million E80's therefore indicated that the pavement was close to the end of its structural service life.

b) Higher than normal deflections occurred at the joints due to heavy loading and a relatively thin concrete slab.

c) Water that entered through the joints that were not watertight caused erosion of the subbase, resulting in voids between the slab and the subbase.

3.4.3 Road Section 2

3.4.3.1 Existing pavement design

Road Section 2 is situated in a wet climatic region (N < 2; Weinert, 1964) in the South African province of Kwazulu-Natal. Chemical weathering of the in situ and pavement materials could therefore be expected as the main mode of deterioration caused by the environment. The asphalt pavement, originally constructed in 1970, was rehabilitated in 1987 by a jointed concrete overlay. No rehabilitation actions, apart from minor resealing of joints have been recorded since 1987. The pavement structure is summarised in Table 3.5 (N3 HS1 PD, 1999).

Test pit investigations confirmed the thickness and quality of the asphalt layer and the crushed stone base. However, no sign of stabilisation of the original subbase could be found, probably due to carbonation action. From a depth of 750 mm and deeper, the pavement is underlain by a mixture of silty and sandy clay of poor quality, less than a G10 Class material (Draft TRH14, 1985).

Table 3.5: Existing pavement of Road Section 2

Layer	Thickness (mm)	Description (year constructed)	CBR values	
			Range	Average
Surfacing	230 80	Jointed Portland cement concrete (1987) Gap-graded asphalt (1970)	-	-
Base	200	Crushed stone (1970)		
Subbase	150	Cement stabilised natural gravel (1970)	-	-
Selected	250	Natural gravel (1970)	14 – 44	32

3.4.3.2 Field investigations

Field investigations included an extensive visual survey, coring the concrete at selected positions, and determining the deflection at joints and mid-slab, as well as RMs at joints with a FWD, as summarised in Table 3.6. The statistics given in Table 3.6 indicate the average, minimum and maximum of the deflection, RM, and the calculated LTE results. The maximum RM, for example, therefore does not necessarily correlate with the maximum LTE. The functional condition of the pavement was determined with an Automatic Road Analyser (ARAN) vehicle.

Table 3.6: Summary of FWD test results on Road Section 2

Direction	Statistics	40 kN Deflection (mm)		RM at joint (mm)	LTE (%)
		Mid-slab	Joint		
Northbound	**Average**	0,083	0,109	0,018	74
	Minimum	0,044	0,052	0,000	13
	Maximum	0,400	0,332	0,187	100
Southbound	**Average**	0,098	0,093	0,028	78
	Minimum	0,036	0,064	0,002	20
	Maximum	0,805	0,207	0,121	100

From the visual survey, it could be concluded that the pavement structure was generally in a good condition with isolated areas showing distress such as cracking, pumping and spalling. There was only one construction related problem that was identified in the visual survey, namely, double saw-cutting of longitudinal joints at places. The conditions of the crack and joint seals varied from fair to poor which, if not maintained properly will be to the detriment of the joint behaviour.

A core drilled at a position where faulting of approximately 15 mm occurred showed signs of dirt and mud washed into the crack. On the other hand, the majority of cores taken at sawn joints showed little signs of distress with good aggregate interlock load transfer. It was difficult to determine the in situ joint width, as this required specialised drilling techniques.

3.4.3.3 Structural evaluation and remaining life

The FWD test results were analysed with Evercalc to determine the elastic moduli of the existing pavement layers. The RM of the pavement was determined with Kenslabs (Huang, 1993). The results of the modelling are summarised in Table 3.7.

Table 3.7: Modelling of the concrete pavement structure

Direction	Back-calculated elastic modulus (MPa)			RM -Kenslabs (years)
	Slab	Subbase	Subgrade	
Northbound	36 700	1 600	180	14
Southbound	37 800	1 650	175	15

The future rehabilitation strategy proposed for this pavement at the time of investigation was to maintain the pavement by replacing joint seals and conducting minor repairs for approximately 14 years. Thereafter minor concrete repairs, and a stress absorbing membrane interlayer (SAMI) combined with a 40 mm asphalt overlay was proposed.

3.4.4 Road Section 3

3.4.4.1 Existing pavement design

The pavement of Road Section 3 was constructed in 1978 as a jointed concrete pavement with asphalt shoulders. This road section is situated in a wet to moderate climatic region (5 > N > 2, Weinert, 1964) in the South African province of Kwazulu-Natal. A combination of both chemical and mechanical weathering of the in situ and pavement materials could therefore be expected as the mode of deterioration caused by the environment. Minor rehabilitation works were carried out during 1991 when the joint sealant was replaced, cracks sealed and distressed areas on the asphalt shoulder repaired by patching with new asphalt. Minor repair works were also carried out on the concrete during 1998 as part of routine maintenance. The existing pavement structure is summarised in Table 3.8 (N3 HS4 PD. 1999).

Test pit investigations in the asphalt shoulders showed that the asphalt layer was approximately 50 mm thick. The pavement as-built data indicated cement stabilised crushed stone subbase layers, but during the test pit investigations it was found that the concrete lies on top of two stabilised decomposed dolerite layers, each approximately 200 mm thick. Below the two stabilised layers the material is a mixture of decomposed dolerite and shale.

Table 3.8: Existing pavement of Road Section 3

Layer	Thickness (mm)	Description	CBR values	
			Range	Average
Surfacing	210	Jointed Portland cement concrete	-	-
Upper subbase	100	Cement stabilised crushed stone	79 – 93	87
Lower subbase	100	Cement stabilised natural gravel	42 – 53	49
Selected	190	Natural gravel	21 – 41	28

3.4.4.2 Field investigations

Visual surveys indicated that the main defects of the pavement were cracked slabs and the poor condition of the flexible shoulders. The predominant forms of distress in the concrete pavement were as follows:

a) Mid-slab longitudinal cracking, due to the settlement of high fills, as well as the relieving of "kick-out" stresses around horizontal curves in the road.
b) Patches co-existing with longitudinal cracks near transverse joints. The patches were a result of maintenance actions to repair spalling and punch-outs at joints.
c) Transverse cracking occurred to a lesser extent than longitudinal cracks, and was more prevalent at the beginning and end of the section due to the formation of "restraint" stresses.
d) Corner cracking was the least pronounced form of cracking suggesting pumping distress with subsequent creation of voids and corner cracks.

The visual appearance of the shoulders varied greatly. Detail recorded included local structural failures, potholes, crocodile cracks, pumping, transverse cracks, block cracks and deformation. During construction of the pavement a no-fines concrete drain (100 mm wide and 210 mm deep) with a drainage pipe at the bottom was constructed between the outer asphalt shoulder and the concrete on both carriageways. This proved an inefficient measure as the drainage pipe itself initially blocked up, the plastic pipe disintegrated, and the area surrounding the pipe and inside the no-fines concrete got saturated with moisture. It could also be reasoned that failure of the drain occurred due to heavy vehicles travelling partly on the shoulder, but this rarely happened, as investigations showed that the automatic delineation of the white concrete travelling lane against the black asphalt shoulder, kept the vehicles on the concrete itself. The end result was a 350 mm wide failed section in the asphalt shoulder adjacent to the concrete, which necessitated the removal of the no-fines drain and failed asphalt section along the entire length of road, and filling up the trench with dense-graded asphalt.

Instrument measurements carried out during field investigations included determining deflections and RM at joints with a FWD, skid resistance with a SCRIM, and riding quality with an Inertial Profilometer. The functional condition of the pavement was determined with an ARAN. FWD testing was also conducted on the asphalt shoulders. The FWD test results for the concrete pavement are summarised in Table 3.9.

Table 3.9: Summary of FWD test results on Road Section 3

Direction	Statistics	40 kN Deflection (mm)		RM at joint (mm)	LTE at joint (%)
		Mid-slab	Joint		
Northbound	Average	0,095	0,216	0,119	52
	Minimum	0,044	0,065	0,001	11
	Maximum	0,453	0,622	0,554	100
Southbound	Average	0,101	0,225	0,126	85
	Minimum	0,024	0,065	0,002	8
	Maximum	0,598	0,680	0,586	100

3.4.4.3 Structural evaluation and remaining life

The concrete pavement and asphalt shoulder FWD test results were analysed separately to determine the elastic moduli of the existing pavement layers, as well as the RM of each. The results of the modelling are summarised in Tables 3.10 and 3.12.

Table 3.10: Detailed modelling of the concrete pavement structure

Location (km – km)	Maximum deflection 90 percentile (mm)	Back-calculated elastic modulus (MPa)		Modulus of subgrade reaction (MPa/m)
		Slab	Subbase	
Northbound carriageway				
12,3 – 17,8	0,065	16 000	2 500	200
18,0 – 21,8	0,087	18 200	1 800	100
22,0 – 27,6	0,072	16 800	830	140
27,8 – 38,0	0,115	15 350	2 000	50
Southbound carriageway				
12,3 – 17,4	0,080	17 500	1 050	110
17,6 – 24,4	0,074	23 750	2 150	155
24,6 – 33,2	0,104	15 900	1 600	115
33,4 – 38,0	0,101	12 550	1 400	155

Table 3.11: Detailed modelling of the asphalt shoulder pavement structure

Pavement Layer	Average 40 kN deflection (mm)	Average thickness (mm)	Back-calculated elastic modulus (MPa) Average (Range)
Northbound carriageway			
Asphalt surfacing	0,194	50	4 450 (1 000 – 6 500)
Stabilised base		170	1 800 (300 – 4 500)
Stabilised subbase		250	860 (200 – 3 000)
Selected		300	190 (70 – 400)
Subgrade			100 (60 – 160)
Southbound carriageway			
Asphalt surfacing	0,276	50	4 740 (1 500 – 6 150)
Stabilised base		170	1 780 (310 – 4 500)
Stabilised subbase		250	710 (210 – 2 250)
Selected		300	230 (90 – 400)
Subgrade			100 (60 – 160)

The RM of the concrete pavement was determined with Kenslabs (Huang, 1993), a finite element software program that can be used to determine the pavement response under load. The concrete pavement structural capacity was calculated as 7,7 million E80's. The pavement had adequate structural capacity for the estimated traffic loading to last another 6 years, provided that timely maintenance in the form of crack sealing, patching, and replacement of some cracked slabs and poor patches was carried out.

The RM of the shoulders was calculated as 12,5 million E80's in the northbound direction, and 11,9 million E80's in the southbound direction. It was important that the shoulders should also have an adequate RM, as it is part of the maintenance strategy of this specific pavement that, firstly, the entire pavement width be provided with a bitumen rubber single seal, after repairing the no-fines concrete drain, and sealing and repairing the shoulders where necessary. This single seal will then act as a SAMI for the asphalt overlay to be constructed after 6 year's time.

3.4.5 Road Section 4

3.4.5.1 Existing pavement design

Road Section 4 is situated in a moderate climatic region (N > 5; Weinert, 1964), in the South African province of Kwazulu-Natal. Mechanical weathering of the in situ and pavement materials could therefore be expected as the main mode of deterioration caused by the environment. The pavement was constructed in 1988 as a jointed concrete pavement with concrete shoulders. Due to sideways

slipping/settlement of the subgrade across high fills stitching repairs had to be done on longitudinal cracks and longitudinal joints in 1988/1989 already. Apart from that, no major rehabilitation works have been carried out on this pavement since construction. Minor repair works were carried out during 1998 during maintenance activities. The structure of the existing pavement is summarised in Table 3.12 (N3 HS5 PD, 1999).

Table 3.12: Existing pavement structure of Road Section 4

Layer	Thickness (mm)	Description	CBR values	
			Range	Average
Surfacing	210	Jointed Portland cement concrete	-	-
Subbase	100	Cement stabilised crushed stone	-	-
Selected	300	Natural gravel. Top 150 mm lime modified	15 – 18	17

3.4.5.2 Field investigations

From the visual survey, it was concluded that the pavement was generally in a good condition with isolated instances of cracking, pumping and spalling. The condition of the crack and joint sealants varied from fair to poor. Settlement of the subgrade occurred in a few areas (N3 HS5 PrD, 2001).

Construction-related distresses were encountered on the pavement, which necessitated the stitching repair done on the longitudinal cracks and joints during 1988/1989. This was necessary because in some places the tie-bars were not placed beneath the position where the longitudinal joint had to be cut, but next to it. The tie-bars could therefore not perform the function it was meant to. These stitching repairs kept longitudinal cracks from propagating at certain places, but were less successful in other places, especially over high fills. It was found that due to a scarcity of good construction material during construction, materials of poor quality were used in the middle of the fill. Although a shield of better quality material protected these materials some settlement did take place.

The visual distresses on this road could be grouped into six categories, as follows:

a) Widening of longitudinal joints.
b) Corner breaks next to stitches where the stitch over-stressed the concrete, or where the stitch was too close to a transverse joint.
c) Localised settlement of the subgrade over short sections of road at a few locations.
d) Problems related to poor subsoil drainage in some cuts.
e) Transverse and longitudinal cracks occurred randomly, and were considered to be traffic related.

f) Fine shrinkage-related cracks at two bridge (underpass) sites. This was not considered a matter of great concern.

Instrument measurements carried out during field investigations included determining skid resistance using the SCRIM apparatus, determining the functional condition of the pavement using the ARAN, and determining deflections and RMs at joints with FWD testing.

Poor deflection and riding quality results were obtained. Low LTE across joints was attributed to a loss of aggregate interlock. The deflection and RM results at mid-slabs and at joints are summarised in Table 3.13.

Table 3.13: Summary of FWD test results for Road Section 4

Section	Direction	Statistics	40 kN Deflection parameters			
			Deflection (mm)		RM at joint (mm)	LTE at joint (%)
			Mid-slab	Joint		
N3/5 km 38-54	Northbound	Average	0,039	0,071	0,030	84
		Minimum	0,018	0,024	0,000	2
		Maximum	0,068	0,386	0,454	100
	Southbound	Average	0,047	0,068	0,018	83
		Minimum	0,021	0,026	0,002	24
		Maximum	0,163	0,183	0,146	100
N3/6 km 0-29	Northbound	Average	0,044	0,181	0,181	19
		Minimum	0,019	0,050	0,010	1
		Maximum	0,091	0,486	0,537	85
	Southbound	Average	0,044	0,117	0,107	27
		Minimum	0,021	0,043	0,008	2
		Maximum	0,163	0,331	0,341	96
N3/6 km 29-36	Northbound	Average	0,067	0,177	0,159	28
		Minimum	0,028	0,057	0,002	5
		Maximum	0,169	0,451	0,490	100
	Southbound	Average	0,115	0,329	0,256	43
		Minimum	0,025	0,042	0,000	1
		Maximum	0,358	0,975	1,052	100

3.4.5.3 Structural evaluation and remaining life

The FWD test results were analysed using Evercalc back-calculation software to estimate the elastic stiffness values of the various layers of the existing pavement. The RM was also determined with Kenslabs (Huang, 1993), as for the previous section. The stiffness moduli determined for the concrete pavement ranged from 27 700 MPa to 53 000 MPa, and for the subgrade from 185 MPa to 320 MPa.

The concrete pavement structural capacity was calculated as 36 million E80's. The pavement had adequate structural capacity for the estimated traffic loading to last another 20 years, provided that timely maintenance in the form of crack sealing, patching, and replacement of some cracked slabs and poor patches was carried out.

3.5 CONCLUSIONS

The conclusions reached so far from the laboratory studies are as follows:

a) There was no significant deterioration or abrasion of the crack up to 2 million dynamic load cycles at the initial crack width, which indicated that the two sections of the slab were still so tightly knit together that little vertical sliding could take place. As there was little movement of the two parts of the slab relative to each other, fatigue or abrasion of the aggregates at the joint face did not play a role. On the other hand, the horizontal displacement movement did increase during dynamic loading. The fact that the deflections (vertical movement) did not increase can therefore be attributed to the high quality of the crushed stone used in South Africa.

b) An increase in crack width caused an increase in deflection.

c) The larger 37,5 mm aggregate had lower deflections than the smaller 19 mm aggregate at the same crack widths during dynamic and static loading.

d) Moment and inertia in the slab contributed to the greater LTE under dynamic loading, than under static loading.

e) Beyond a crack width of 2,5 mm the data for the 19 mm coarse aggregate tended to remain constant, and it was therefore not considered necessary to test at crack widths greater than 2,5 mm. It was also specifically stated in previous research studies (Davids et al., 1998b; Jensen, 2001) that at crack widths greater than 2,5 mm the stiffness of the subbase starts to play a role in levelling out the measured response of the slabs. However, this study has shown that the smoother the texture of the crack face, the sooner the system would rely on the support of the subbase to transfer stresses and strains from one slab to another. This study has indicated three such transition zones, namely: 1,5 mm for the smooth joint, 2,5 mm for the 19 mm aggregate interlock joint, and between 3,5 mm and 4,0 mm for the 37,5 mm aggregate interlock joint.

f) At small crack widths (< 0,5 mm) the bottom crack displacement measurements tended to be higher than the top crack displacement measurements. The slab tended to bend through with the top of the crack closing, and the bottom of the crack opening during loading. This was more evident during dynamic loading than during static loading, due to the effects of momentum.

g) At crack widths greater than 0,5 mm the top crack displacement became larger than the bottom crack displacement, indicating that the two parts of the slab were being pushed apart during loading. This demonstrated why large crack widths are so detrimental to pavement

performance, as the opening up of the crack at the top during loading, makes it so much easier for debris and loose particles to be driven into the cracks, which in turn cause spalling of the concrete at the crack face. Once again the effect was greater during dynamic than static loading.

h) The deflection LTE was greater during dynamic than static loading in all instances. Larger maximum sized aggregates had greater deflection load transfer efficiencies than smaller maximum sized aggregates.

i) For the same coarse aggregate size concrete mixes, the LTE was larger where there was a continuous rubber support (rubber not cut through) than where there was a crack simulated into the subbase (top rubber layer cut through).

j) Due to the effects of momentum forces acting across the crack, the LTE under 40 kN static loading was higher than under 20 kN static loading.

k) Also due to the effects of momentum acting across the joint, the LTE under dynamic loading of a plastic joint remained remarkably high (92% at a crack width of 2,5 mm), compared to the gradual decrease in LTE with increasing crack width under static loading (18% at a crack width of 2,5 mm).

l) Although the deflections were similar, the load transfer efficiencies achieved using South African crushed stone were significantly higher when compared to published results. The 19 mm dolomite aggregate rendered greater load transfer efficiencies than a 50 mm glacial gravel blend commonly used in the USA.

m) The joint shear stiffness (*AGG*) under dynamic loading was approximately 1,5 times that of the *AGG* under static loading on the continuous rubber subbase, and approximately 3 times higher on the discontinuous rubber subbase.

n) The range of shear stiffness per unit length of crack face that could typically be expected from South African aggregates under static loading has been established.

o) Logistic regression equations were fitted to the data in terms of relative movement (y) versus crack width (x) for both 19 mm and 37,5 mm, maximum sized aggregate. These functions apply to the relative movement induced at a joint/crack by each wheel of an 80 kN dual wheel truck axle crossing the joint/crack.

The laboratory and the field data are analysed in more detail in the next chapter (Chapter 4).